



Brown carbon emissions from laboratory combustion of Eurasian 1

arctic-boreal and South African savanna biomass 2

Arya Mukherjee¹, Anni Hartikainen¹, Markus Somero¹, Viljami Luostari¹, Mika Ihalainen¹, Christopher P. Rüger², Timo Kekäläinen³, Ville H. Nissinen³, Luis M.F. Barreira⁴, Hanna Koponen¹, 4

- 6
- 7
- Tuukka Kokkola¹, Delun Li^{4,9}, Lejish Vettikkat⁵, Pasi Yli-Pirilä¹, Muhammad Shahzaib¹, Meri M. Ruppel⁴, Ville Vakkari^{4,6}, Kerneels Jaars⁶, Stefan J. Siebert⁷, Angela Buchholz⁵, Kajar Köster⁸, Pieter G. van Zyl⁶, Hilkka Timonen⁴, Niko Kinnunen³, Janne Jänis³, Annele Virtanen⁵, Aki Virkkula^{4,9}, Olli 8
- 9

3

10

24

25

11 ¹ Department of Environmental and Biological Sciences, University of Eastern Finland, Kuopio, Finland

- 12 ²Joint Mass Spectrometry Centre, Department of Analytical and Technical Chemistry, University Rostock, Rostock, 13
- 14 ³Department of Chemistry and Sustainable Technology, University of Eastern Finland, Joensuu, Finland.
- 15 ⁴Atmospheric composition research unit, Finnish Meteorological Institute, Helsinki, 00101, Finland
- 16 ⁵Department of Technical Physics, University of Eastern Finland, Kuopio, Finland. 17 ⁶Atmospheric Chemistry Research Group, Chemical Resource Beneficiation, North-West University, Potchefstroom,
- 18
- 19 ⁷Unit for Environmental Sciences and Management, North-West University, Potchefstroom, South Africa.
- 20 ⁸Department of Environmental and Biological Sciences, University of Eastern Finland, Joensuu, Finland.
- 21 ⁹Institute for Atmospheric and Earth System Research, University of Helsinki, Helsinki, 00014, Finland 22
- 23 Correspondence to: Arya Mukherjee (arya.mukherjee@uef.fi) and Olli Sippula (olli.sippula@uef.fi)

Abstract:

- 26 Warming climate is predicted to increase forest fires which can be a major source of black and brown carbon
- 27 (BC and BrC) into the atmosphere. Unlike North American forest fires, very limited studies have
- 28 characterized North Eurasian biomass burning (BB) emissions. In this work, we defined the emission factors
- 29 of carbonaceous aerosols and characterized light absorption of BrC emitted from boreal and peat burning
- 30 through offline filter extraction method. The results were compared to African savanna emissions. Effects of
- 31 atmospheric dilution and oxidative aging on BrC absorptivity were investigated for selected BB emissions
- 32 sampled into an environmental chamber. Organic carbon (OC) and elemental carbon (EC) emission factors
- of fresh BB emissions ranged between 1.30-89.9 g kg⁻¹ and 0.01-4.80 g kg⁻¹ respectively. Methanol soluble 33
- 34 OC (MSOC) represented more than 92% of fresh BB emissions but intrinsic chemical differences among
- 35 samples resulted in MAC_{MSOC} values ranging from 0.46-1.48 m² g⁻¹ at 365 nm. Fresh BB emissions formed
- 36 weakly absorbing BrC with k_{550 MSOC} ranging from 0.002 and 0.011. Water soluble OC (WSOC) fractions
- 37 varied among fresh BB emissions but overall exhibited higher MAC₃₆₅ than MSOC. Dilution-related





evaporative loss in environmental chamber resulted in less volatile OC, making them less soluble in methanol. Photochemical and dark oxidative aging further increased the ELVOC fraction of the organics along with oxidation state. Our estimated OC-EC emission factors and k_{MSOC} for fresh BB emissions can be used for future modelling purposes. Further online measurements are needed to account for non-soluble strong BrC in aged BB emissions.

43 44

45

64

38

39

40 41

42

Introduction:

46 Biomass burning (BB) emission is one of the largest anthropogenic sources of black (BC) and brown carbon 47 (BrC) in the atmosphere (Bond et al., 2004; Kirchstetter et al., 2004). Multiple studies have predicted that 48 open BB emissions such as wildfires will become more prevalent in the future with the warming climate, 49 with increasing boreal forest and peatland fires threatening also the Eurasian regions (Krawchuk et al., 2009; 50 Costa et al., 2020; Feyen et al., 2020). Along with the expected overall increase in the frequency of "high-to-51 extreme" wildfires in Europe (de Rigo et al., 2017) an expected shift in vegetation distribution from Southern 52 towards Northern Europe might add stress on Finno-Scandinavian biomass and amplify its fire hazard (Costa 53 et al., 2020). Only limited laboratory and field studies exist describing aerosol emissions from boreal forest 54 and peatland fires in the Eurasian area (Wilson et al., 2015;McCarty et al., 2021;Zhong et al., 2024; 55 Schneider et al., 2024a), compared to the more studied North-American boreal forest and peat fires (Aurell 56 and Gullett, 2013; Urbanski, 2013; Stockwell et al., 2014; Black et al., 2016; Andreae, 2019; Phillips et al., 57 2022; Zhao et al., 2021). However, the fire regimes in Eurasia are known to be dominated by surface 58 burning, that likely emits carbonaceous aerosol of different characteristics in comparison to more crown-fire 59 dominated fires in North America (De Groot et al., 2013; Rogers et al., 2015). 60 Chemical and optical properties of BC have been studied extensively over the last two 61 decades and it has been established as an important climate warming agent (Jacobson, 2000, 2001; Bond et 62 al., 2013). On the other hand, the properties of combustion emitted BrC have still not been fully 63 characterized due to variability in combustion conditions (Martinsson et al., 2015; Wang et al., 2020; Saleh,

2020), fuel chemical composition (Saleh et al., 2014; Smith et al., 2020; Moschos et al., 2024; Navinya et al.,





65 2024) and secondary transformation of BrC in the atmosphere (Laskin et al., 2015; Brown et al., 2018; Hems 66 et al., 2021). BB derived BrC consists of different light-absorbing organic precursors of BC, such as 67 polyaromatic molecules, which are not transformed to fully ordered BC during the combustion process 68 (Saleh et al., 2018). Since BC formation is strongly temperature-dependent, low combustion temperatures 69 may favour BrC formation, whereas high combustion temperatures increase oligomerization/polymerization 70 of polyaromatic carbon structures to form BC (Faccinetto et al., 2011; Desgroux et al., 2013; Solum et al., 71 2001; Wang, 2011). Consequently, the light-absorbing primary organic aerosols (POA) emitted from BB 72 emission are chemically diverse and distinct for different fuel types and combustion conditions. Additionally, 73 they evolve in the atmosphere through oxidation and functionalization reactions, driven by the formation of 74 secondary organic aerosol (SOA) and the evaporation and chemical fragmentation of organic aerosol (OA), 75 resulting in a complex mixture of organic chromophores with variable absorptivity. 76 BB is a dynamic and variable process that strongly depends on fuel moisture content, fuel 77 composition and combustion conditions. A common parameter to characterize BB is the modified 78 combustion efficiency (MCE), which describes the share of carbon dioxide to the sum of CO and CO2 79 emissions. However, studies have typically found only weak correlations between BrC light absorption and 80 MCE (Pokhrel et al., 2016; McMeeking et al., 2014). The ratio of the emitted BC (mainly composed of 81 elemental carbon or EC structures) to the organic carbon (OC) has been suggested as a more suitable 82 parameter for correlating the aerosol optical properties with combustion conditions (McClure et al., 2020; 83 Stockwell et al., 2016; Saleh, 2020). For instance, flaming dominated combustion processes generally lead to 84 relatively high EC/OC ratios and more absorptive BrC than smouldering emissions (Saleh et al., 2014; Xie et 85 al., 2018; McClure et al., 2020; Kumar et al., 2018). 86 In climate models, the light absorption strength of the material is described by the imaginary 87 part of the refractive index (k). For pure BC, k- are constrained close to unity and exhibit very little to no 88 wavelength dependence, especially at UV and shorter visible wavelengths (Bond and Bergstrom, 2006). 89 However, the k for BB emitted BrC seem to vary across several orders of magnitude depending on the 90 biomass type and combustion conditions as well as the measurement techniques (Chakrabarty et al., 2010; 91 Bluvshtein et al., 2017; Saleh et al., 2018; Saleh et al., 2020; Navinya et al., 2024). Therefore, characterizing



93

94

95

96

97

98

99

100

101

102

103

104

105

106

107

108

109

110

111

112

113

114

115

116

117

118



the *k* for individual BrC compounds is a daunting and, in some cases, impossible task due to instrumental limitations. A more comprehensive approach has been adapted in the last decade where the *k* values for BB derived BrC has been shown to fall in a "brown-black carbon continuum" (Saleh et al. 2018). BB derived BrC generally exhibit progressively higher *k* values with increasing temperature, and has been termed as "dark BrC (d-BrC)" (Hoffer et al., 2017; Adler et al., 2019; Atwi et al., 2022; Chakrabarty et al., 2023) or "strongly absorptive BrC (s-BrC)" (Mclure et al., 2020; Saleh et al., 2020) when the combustion temperatures approach the BC formation regime. In contrast, the BrC derived from BB combustions in progressively decreasing combustion efficiency and temperature has been termed as "moderately absorptive (M-BrC)", "weakly absorptive (w-BrC) and "very weakly absorptive (VW-BrC)", respectively (Saleh et al., 2020; Moschos et al., 2024), as the *k* values decrease with lower burning temperature.

One of the most convenient and widely used methods for the characterization of optical

properties of bulk BrC is the collection of aerosol particles on filters and subsequent extraction of the organic fractions with suitable solvents followed by filtration (Chen and Bond, 2010; Liu et al., 2013; Mo et al., 2017; Shetty et al., 2019; Li et al., 2020, Yan et al., 2020). The light absorption of solvent extracted OA is measured using a UV-vis spectrophotometer which provides high precision spectral data over a wide wavelength range. In previous studies water has been one of the primary solvents for extraction of BrC from filters (Bosch et al., 2014; Kirillova et al., 2014; Mukherjee et al., 2020) because of the atmospheric relevance of the water soluble organic (WSOC) fraction (Hallar et al., 2013, Taylor et al., 2017). Quantification of WSOC can be done with Total Organic Carbon (TOC) analysis (Li et al., 2016), and the loss estimation of the extraction process has very little uncertainty. On the other hand, the water insoluble BrC fraction is generally extracted from aerosol particles using methanol (MeOH) as a solvent (Chen and Bond, 2010) but it has been recently discovered that some highly light-absorbing, extremely low volatility organic (ELVOC) compounds may not be efficiently extracted by this procedure (Saleh et al., 2014; Liu et al., 2013). Quantifying the dissolved organic mass in MeOH is also challenging as organic solvents interfere with TOC measurements and indirect methods are used instead (Chen and Bond 2010; Cheng et al., 2017; Huang et al., 2018; Yan et al., 2020) to estimate methanol soluble organic carbon (MSOC) which leads to additional potential sources of uncertainties (Yan et al., 2020). Nevertheless, MeOH has exhibited very high



120

121

122

123

124

125

126

127

128

129

130

131

132

133

134

135

136

137

138

139

140

141

142



organic extraction efficiencies (Chen and Bond, 2010; Xie et al., 2017) and the optical properties of MSOC have agreed well with OC extracted by more polar solvents like Dimethylformamide (DMF) for BB emissions and coal combustion (Xu et al., 2022). Therefore, MeOH should be used in parallel to water to extract BB emitted organic compounds with a broader range of polarities and gain more information on their light-absorbing properties. Although filter based solvent extraction has its limitations, such as lack of information on size-dependent absorption of extracted organics (Moosmüller et al., 2011; Liu et al., 2013; Washenfelder et al., 2015), this analytical method is low-cost, easily accessible, and excludes the interference of BC (or EC) and other light-absorbing species from OA absorption.

This work aims to define the emission factors of carbonaceous aerosols and characterize OA optical properties for emissions originating from different open BB sources. We used a laboratory open burning setup with the objective to create conditions representing natural Eurasian forest surface fires, in which the combustion temperatures likely remain low and burning is dominated by smouldering (Rogers et al., 2015; Walker et al., 2020). Finnish boreal peat and forest surface samples, commercially available boreal peat samples, and permafrost peat from arctic Russia and Svalbard (Norway) were burned in the laboratory setup. To assess the effects of burning conditions and biomass materials on carbonaceous emission factors and their optical properties, we replicated conditions ranging from smouldering to flaming, with clearly distinct combustion behaviour and MCEs for each fuel. Furthermore, we extended the study samples to include South-African savanna biomass and North European wood stove emissions, thereby encompassing a larger range of combustion conditions. Finally, we investigated the impact of atmospheric dilution and aging on the chemical and optical properties of the organic aerosols by conducting environmental chamber experiments either under photochemical or dark aging conditions for selected biomasses. The results were used to derive imaginary refractive indices (k) for OAs, allowing for their classification within the blackbrown carbon continuum. The results are essential to accurately estimate the direct radiative forcing effects of biomass burning emissions in climate models.

143

2. Methodology:

144145146

2.1 Combustion setup and fuels





147 The combustion experiments were conducted in the ILMARI laboratory of the Kuopio campus of University 148 of Eastern Finland (https://sites.uef.fi/ilmari) using an in-house designed open combustion appliance. The 149 appliance consisted of a steel cage, a concave plate, a metal/steel mesh and a metal/steel biomass holder. The 150 details of the combustion setup and the specific biomass holders used for each fuel type are illustrated in 151 Supplementary Fig. S2. Combustion was initiated using an electric resistor of which the power was adjusted 152 to generate exclusively 'flaming' or 'smouldering' emissions. 153 Eight different types of biomass were used as fuel samples in the combustion experiments. Namely, 154 commercially available peat samples (CP), Finnish boreal forest surface (BFS, including vegetation, litter, 155 and the soil organic layer), peat from two Finnish boreal peatlands (FIA and FIB), peat from arctic 156 permafrost regions of Russia (RUS) and Norway (NOR), savanna wood and grass from South Africa (SW 157 and SG respectively) were selected as fuels for this study. The origins and properties of the combusted 158 biomasses are available in the Supplementary Information (Section S1, Table S1). The savanna biomass 159 included in this study was part of the BASFAA (Boreal and savanna fire aerosol aging) measurement 160 campaign that took place from May to June 2022 at the ILMARI laboratory as described in Vakkari et al. 161 (2025). For this study specific combustion phases were selected for sampling representing either solely 162 flaming, pre-flame smouldering, or full combustion consisting of pre-flame smouldering, flaming and post-163 flame smouldering periods. Therefore, a subset of Savanna biomass (SG and SW) combustions presented in 164 Vakkari et al. (2025), which included sampling of separate combustion phases (either flaming or pre or post 165 flame smouldering), were chosen to be included in this study. The sampling periods were selected based on 166 careful visual inspection of the combustion process and the concentrations of CO and CO2, monitored online 167 as described below (Section 2.2). 168 2.2. Sampling setup and gas phase measurements

2.2. Sumpling secup and gas product measurements

169 The emitted smoke was sampled using the setup presented in Fig. 1. We measured the gaseous

170



173

174 175

176

177

178

179

180

181



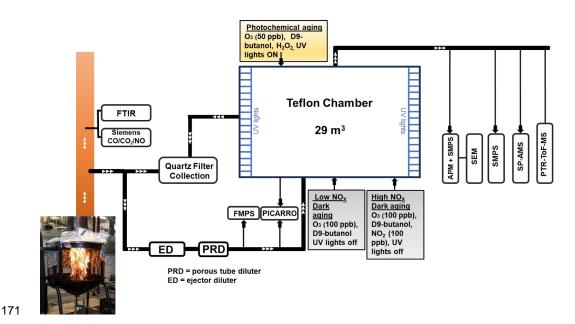


Figure 1: A schematic presentation of the experimental setup for combustion experiments involving the environmental chamber

compounds from the fresh, undiluted BB emission using an online multicomponent FTIR analyzer (Gasmet Technologies Inc.), and the measured compounds are listed in Table S2. The fresh BB emissions were sampled through a PM₁₀ pre-cyclone and a heated probe (180 °C) before being diluted using an Ejector Dilutor (Titta et al., 2016) and porous tube dilutor (PRD). A dilution ratio (DR) of 4-20 was achieved during this two-stage dilution with clean synthetic air (Woikoski N50) in ambient temperature. A gas concentration analyzer (Picarro G2401) measured the concentrations of CO₂, CO, CH₄ and water vapor (H₂O) from the diluted exhaust (Fig. 1).

MCEs were calculated from the average increase in CO₂ and CO concentrations during the sampled combustion period relative to the background concentrations (Eq. 1)

184
$$MCE = \frac{\Delta[CO_2]}{\Delta[CO_2] + \Delta[CO]}$$
 (1)

185 MCE was estimated from CO and CO₂ concentrations measured in both undiluted and diluted BB emission.

186 Burns with average MCE values smaller than 0.9 were defined as smouldering-dominated combustion, while





the combustions with average MCE values larger than 0.9 were classified as flaming dominated (Table 1).

188

189

190

191

192

193

194

195

196

197

198

199

200

201

202

203

204

205

206

207

208

209

210

211

212

213

187

2.3 Environmental chamber and aging of the emissions

Different burning phases of Finnish BFS, and Finnish commercial peat (CP) samples were used in the chamber experiments to study the effects of dilution and oxidative aging on the organic aerosol optical properties. Additionally, samples of Savanna burning chamber experiments, described by Vakkari et al. (2025), were analyzed as part of this study. For peatland samples FIA, FIB, NOR and RUS, only fresh emissions were characterized in this study and no chamber feeding was performed. In each of the chamber experiments, diluted primary BB emissions were sampled into a 29 m³ TeflonTM chamber (Leskinen et al., 2015) which was pre-filled with purified air (Model 737-250, Aadco Instruments Inc.). For each experiment, the sampling period to the environmental chamber was set based on the targeted mass concentration of 20-50 μgm⁻³ as estimated from the fresh particle size distribution measured online by a fast mobility particle sizer (FMPS, model 3091, TSI Inc.). The relative humidity (RH) inside the chamber was maintained at 20% for SG and SW emissions and at around 50% for BFS and CP emissions to reproduce typical daytime RH in corresponding environments during the fire active seasons. The temperature in the chamber was kept constant at approximately 22°C. The sample was first allowed to mix and homogenise for 20 minutes, which was an adequate duration for the mass concentrations of particulate matter (PM) and organics inside the chamber to stabilize, as observed respectively by a scanning mobility particle sizer (SMPS) and a soot particle aerosol mass spectrometer (SP-AMS, Aerodyne Research Inc, USA) connected to the chamber. After sampling of the fresh exhaust, Picarro was switched to monitor the gaseous components inside the chamber. Total DRs inside the chamber were 135-4045 compared to the two-stage diluted fresh emission (Table 1), based on the ratio of CO concentration measured by Picarro in the diluted exhaust and from the chamber.

After the stabilization period, chamber diluted primary BB emissions were monitored for additional 45 mins before adding reactants to the chamber to induce oxidative aging. The reactants were allowed to interact with the fresh BB emission in the chamber for 4.5 hours. For each experiment, 2 µL of d9-butanol (~25 ppb) was injected into the chamber and the concentration was probed throughout the experimental duration using a proton-transfer-reaction time-of-flight mass spectrometer (PTR-ToF-MS).



240



215 on the physio-chemical and optical properties of different BB emissions. Firstly, photochemical aging 216 conditions were induced inside the chamber for both flaming and smouldering combustion. In the 217 photochemical experiments, UV-light in presence of externally fed O₃ (50 ppb) and H₂O₂ (0.5 ml of 30% v/v 218 solution) led to the formation of hydroxyl radicals (OH·). The OH exposure and equivalent photochemical 219 age were determined from the decay of d9-butanol (Barmet et al., 2012). In our experiments, equivalent 220 photochemical age ranged between 1-1.6 days (Table 1) with an assumed ambient OH concentration of 221 1.5×10⁶ cm⁻³. In addition, two different dark aging conditions were simulated for two distinct sets of biomasses. The primary emissions from SG and SW underwent dark aging in the presence of externally 222 223 added 100 ppb of O₃ and no additional NO_x. We classified this aging condition as "low-NO_x dark aging", as 224 the nitrate radical (NO₃) formation was limited by the lack of NO₃. CP and BFS burning emissions were 225 aged in relatively 'high-NO_x' conditions in the dark chamber with 100 ppb O3 and 100 ppb NO₂ added 226 externally. It should be clarified that even though we termed this aging condition as "high- NO_x ", the 227 NMVOC/NO_x ratio was still relatively high (Seinfield and Pandis, 2006) in the range of 4-6 in these cases 228 (Table 1). Furthermore, seven experiments were conducted without any added oxidants in the chamber to 229 evaluate the impacts of chamber dilution and other chamber processes on the exhaust emissions. Out of these 230 seven experiments three were conducted by sampling emissions from the whole combustion of BFS, while 231 the other four experiments were constituted with distinct smouldering and flaming dominated burns of CP 232 and BFS. 233 2.4 Particle size distribution, density and morphology: 234 The particle size distributions were measured from the environmental chamber for the whole duration of 235 each experiment by a scanning mobility particle sizer (SMPS) consisting of a differential mobility analyzer 236 (DMA, model 3080; TSI Inc.) and a condensation particle counter (CPC, model 3775; TSI Inc.). In addition, 237 an aerosol particle mass analyzer (APM, model 3602; Kanomax Inc.) in tandem with another SMPS (with 238 DMA 3081 and CPC 3750, TSI Inc.) was used to measure the size distribution of mass classified particles to 239 estimate the size-resolved effective densities of the particles (Leskinen et al., 2023; Mukherjee et al., 2024).

Four distinct aging conditions were simulated in the environmental chamber to evaluate the impact of aging

Particle densities of primary emission from the chamber were measured before the application of any





241 additional reactants to the chamber. The density of the aged particles in the chamber were measured 4.5 242 hours after the addition and stabilization of the reactants (for dark aging) and/or turning on of the UV lights 243 (for photochemical aging; Table S4). Simultaneous to the density measurements, particles were collected on 244 holey-carbon grids (S147-4 Holey carbon film 400 Mesh Cu; Agar Scientific Inc.) from the chamber using 245 an aspiration sampler at a flowrate of 0.3 litres per minute (lpm). Subsequently, we performed Scanning 246 Electron Microscopy (SEM, Sigma HD/VP; Carl Zeiss NTS) to investigate the morphology of both chamber 247 diluted primary and aged BB emitted particles. 248 2.5 Offline optical analyses: 249 Biomass burning emissions were collected on precombusted 90 mm Quartz microfiber filter (PallflexTM 250 TissuquartzTM 7203, Pall Corporation) from the fresh emissions and at the end of each chamber experiment. 251 First, the freshly emitted particles from the raw exhaust without any additional dilution were deposited on the 252 filter at a flow rate of 90 lpm. For experiments with subsequent chamber study, the sampling was done for 253 the same duration as the chamber feed (Fig.1). Approximately 4.5 hours after the chamber feeding, another 254 filter sample was collected from the chamber with the same flow rate for 120 minutes. For the boreal (FIA 255 and FIB) and arctic peat (RUS and NOR) samples, the primary emission was deposited on the filter 256 throughout the whole combustion period, and no chamber studies were performed. 257 258 Thermal-optical analyses were conducted on 1.5 cm² punches of the Ouartz fiber filters (QMA) 259 containing deposited aerosol particles with the IMPROVE-A protocol (Chow et al., 2007) in an OC-EC 260 analyzer (Lab OC-EC Aerosol Analyzer; Sunset Laboratory Inc.). Additionally, two separate filter punches 261 from each experiment were extracted, one with ultrapure Mili-O water (>18.2 M Ω) and the other with 262 methanol (Fisher Scientific, Analytical Reagent Grade >=99.9% pure). After solvent extraction, the two 263 filters were dried under gentle airflow in a clean room for 12 hours before being analysed with the same OC-264 EC analyzer. This setup (Fig. S4) enabled us to measure the dissolved organic concentration in the solvent 265 using Eq. 4 (see section 2.8) and therefore estimate the MAC $_{OC}$ (Eq. 3).





Table 1: List of chamber experiments with detailed parameterization of combustion and aging conditions (mean ± standard deviation)

No.	Fuel	Fuel Combustion	MCE	OC EF (fresh	EC EF (fresh	Final DR	SMPS PM ₁ EF (g	GMD	Aging condition	NMVOC/NO _x	OH exposure	eqv. age
		Condition		emission)	emission)	(chamber)	kg ⁻¹) (chamber	(mm)	(in chamber)	(ppbC/ppb)	(x 10 ¹¹ molecules.cm ⁻³ . s ⁻¹)	(days)
		(no. of replicates)		(g kg ⁻¹)	(g kg ⁻¹)		primary)					
la	CP	flaming (n = 2)	0.971 ± 0.004	5.34 ± 2.32	0.29 ± 0.08	247 ± 106	6.98 ± 4.01	52.4 ± 1.60	photo aged	21.4 ± 4.40	2.09 (± 0.33)	1.61 ± 0.26
116		flaming $(n = 1)$	0.979	1.85	0.40	229	3.86	48.0	high NO _x dark aged	5.45	NA	
lc		flaming $(n=1)$	986.0	1.39	1.81	273	8.05	54.4	no aging	6.40	NA	
1d		smouldering (n = 2)	0.619 ± 0.147	58.3 ± 31.5	0.24 ± 0.07	764 ± 118	152 ± 89	48.3 ± 5.20	photo aged	88.6 ± 5.01	1.15 (± 0.63)	0.88 ± 0.48
le		smouldering (n = 1)	0.793	26.8	0.16	429	33.6	45.5	high NO _x dark aged	4.20	NA	
1f		smouldering (n = 1)	0.479	73.7	0.49	999	228	59.7	no aging	108	NA	
2a	BFS	flaming $(n = 3)$	0.922 ± 0.003	3.20 ± 0.94	0.43 ± 0.15	309 ± 199	6.07 ± 1.05	51.0 ± 4.10	photo aged	63.9 ± 41.7	1.80 (± 0.34)	1.39 ± 0.26
2b		flaming $(n = 3)$	0.952 ± 0.005	3.18 ± 0.70	0.39 ± 0.08	387 ± 140	4.79 ± 0.82	51.6 ± 0.70	high NO _x dark aged	4.78 ± 1.23	NA	
2c		flaming (n = 1)	0.961	3.06	0.73	833	5.95	53.6	no aging	20.0	NA	
2d		smouldering (n = 3)	0.759 ± 0.020	23.9 ± 15.7	0.08 ± 0.07	276 ± 100	48.3 ± 29.5	84.7 ± 41.4	photo aged	133 ± 104	1.57 (± 0.11)	1.21 ± 0.09
2e		smouldering (n = 3)	0.761 ± 0.017	24.0 ± 10.5	0.07 ± 0.06	287 ± 123	26.6 ± 21.1	73.2 ± 22.8	high NO _x dark aged	23.5 ± 19.6	NA	
2f		smouldering (n = 1)	0.774	15.3	0.33	135	23.96	51.2	no aging	163	NA	
За	SW	flaming $(n = 1)$	0.935	8.04	0.97	922	12.4	60.5	photo aged	26.1	1.41	1.09
36		flaming $(n = 1)$	0.950	5.93	09:0	244	10.5	48.0	low NO _x dark aged	43.9	NA	
3c		smouldering (n = 1)	0.589	87.0	5.18	389	61.1	81.0	photo aged	53.2	1.29	0.99
3d		smouldering (n = 1)	0.892	22.5	1.36	416	31.1	62.6	low NO _x dark aged	2.69	NA	
4a	SG	flaming (n = 1)	0.943	4.83	0.31	512	6.24	48.1	photo aged	124	1.46	1.13
46		flaming (n = 1)	0.973	2.87	0.28	1974	5.44	50.3	low NO _x dark aged	2.73	NA	
4c		smouldering (n = 1)	0.803	31.8	1.19	4045	28.6	60.5	photo aged	19.3	1.49	1.15
		smouldering $(n = 1)$	0.843	14.0	1.25	902	23.2	58.5	low NO _x dark aged	108	NA	

 $\stackrel{\leftarrow}{\vdash}$





269 For filters containing fresh emissions collected from the raw exhaust, 40 mL of solvent was used for the 270 extraction of the 1.5 cm² filter area. The volume of solvent used for extraction of highly loaded filters 271 containing fresh emissions can be a limiting factor for dissolved OC concentration, especially for BB emitted 272 particles that have been shown to be dominated by non-polar molecules (Lin et al., 2017) that are less soluble 273 in water. We chose 40 ml of solvent, as this volume provided a dilute micromolar solution in which the light 274 absorption by the dissolved organics would be linearly proportional to their concentration, in accordance 275 with Beer-Lambert's law (Huang et al., 2018). The utilized solvent volume was also sufficient to dissolve the 276 sparingly soluble low volatility strongly light-absorbing fraction of OC. On the other hand, for the chamber 277 diluted fresh emissions and aged particles, 3 cm² filter punches were extracted in 20 mL water or methanol 278 (Cao et al., 2021; Fan et al., 2018) to obtain solution phase organic concentrations necessary for analytically 279 significant S/N ratio in the UV-vis spectrophotometry. 280 In parallel to the deposition of primary particles from the raw exhaust on quartz fiber (QMA) filters for 281 emission factor calculation, a fraction of the emitted particles was fed to the TeflonTM chamber to create real 282 life atmospheric dilution. It is important to study these particles in a diluted system to understand their 283 chemical and optical evolution in the atmosphere. The particle size distribution, effective density, and 284 morphology of the primary BB emission were studied after feeding them in the chamber and letting them 285 mix homogeneously with clean air. Subsequently, different oxidants were added to the chamber to initiate 286 photochemical or dark oxidation reactions. After 4.5 hours of feeding the oxidants, the particles from the 287 chamber were deposited on another OMA filter. In addition to that, five separate experiments were conducted 288 for different BB emissions, where no oxidants were added externally to the chamber and the primary 289 particles were on QMA filter 4.5 hours after the chamber feed. These samples are referred to as "chamber 290 primary" samples. The QMA filters containing chamber aged and chamber primary particles were produced 291 to undergo OC-EC analyses and solvent extraction similar to the QMA particles collecting raw exhaust 292 primary particles. 293 The filter punches were submerged in the solvents and sonicated for 10 mins in three separate intervals in an 294 optimized ultrasonicator (SONOREX Digitec, Bandelin Inc.). The optimization enabled a much gentler 295 sonication as compared to regular commercial ultrasonicators (Huang et al., 2018; Li et al., 2020), resulting





319

320

321

322

297 analyses. Such gentle ultrasonication also minimised the dislodging of insoluble organics or EC from the 298 filter to the solution (Phillips and Smith, 2017). During the intervals between the 10-minute sonication 299 windows, the samples were kept in a refrigerator to keep the effects of any thermal disintegration of OC or 300 chemical transformation through reactions with the solvent (Bateman et al., 2008; Chen et al., 2022) due to 301 the added kinetic and thermal energy during the sonication at minimal. 302 After the sonication, the elute was passed through 0.2 um hydrophilic PTFE syringe filters (Fisherbrand) to 303 remove any insoluble particles from the solution. Aliquots of 3 mL from the filtered solutions were taken in a 304 quartz cuvette with 1 cm path length and UV-vis spectra were recorded for the wavelength range of 250-700 305 nm using a spectrophotometer (UV-2401 PC, Shimadzu). The overall contact time between the solvent and 306 the extracted organics in the solution never exceeded 2 hours before the recording of the optical spectra. 307 These were much smaller time intervals compared to the reaction rates between methanol and carboxyl 308 groups for instance (McIntyre and McRae, 2005), enabling us to disregard any potential artifact caused by 309 the solvent (methanol) to the chemical composition of the original OC deposited on the filter (Lin et al., 310 2012). 311 2.6. Residential wood combustion experiments 312 In addition to different open BB emissions, filter samples from experiments performed with modern 313 European logwood-fired chimney stove (Aduro 9-3) operated with beech logs from two separate 314 experimental campaigns were included in the study. This enabled us to extend the analysed sample set to 315 conditions representing high-temperature biomass combustion, and to test the validity of the BrC-BC 316 continuum. The general experimental setups of these two sets of experiments have been presented in our 317 previous works (Ihalainen et al., 2019a, Mukherjee et al., 2024). Each experiment consisted of four 318 (Ihalainen et al., 2019a) or six (Mukherjee et al., 2024) 45 min batches of wood log burning, ignited with

in high extraction efficiencies without damaging the filter punch and thereby allowing subsequent OC-EC

collected onto quartz fiber filters before and after the PEAR in a flow rate of 10 lpm for 60 min, with each

wood sticks as kindling. Photochemical aging of the residential wood combustion (RWC) exhaust was

conducted by the Photochemical Emission Aging flow tube reactor (PEAR, Ihalainen et al., 2019b), in

similar conditions as the low-dilution aging in Hartikainen et al. (2020). Briefly, exhaust samples were





- 323 sample consisting of one full batch and 20 min of the subsequent batch, either from the cold stove (consisting
- 324 of 1st and 2nd batch of wood) or in the warm stove (consisting of 3rd and 4th batches of wood) combustion.
- 325 The filter samples were extracted similarly to the open biomass burning samples for optical analyses.
 - 2.7. Optical data processing:
- 327 The raw absorption (A) of the extracted solution measured by the UV-vis spectrophotometer was converted
- 328 to the light absorption coefficient (β_{abs} , Mm⁻¹) in the sampled air using Eq. 2 (Hecobian et al., 2010):

329
$$\beta_{abs}(\lambda) = \frac{(A_{\lambda} - A_{700}) \times V_l \times \ln(10)}{V_a \times l}$$
 (2)

- 330 where A_{λ} is the raw absorbance measured by the spectrophotometer in base-10 at wavelength λ and A_{700} is
- 331 the absorption at 700nm (which was subtracted from A_{λ} to correct for baseline drift caused by the
- 332 absorption), V_l is the volume of the extract, V_a (m³) is the volume of the air sampled through the quartz filter
- 333 during emission measurements, *l* is the path length of light through the solution, which is equivalent to the
- width of the quartz cuvette (0.01 m).:
- The mass absorption coefficient (MAC) of the extracted BrC at a particular wavelength λ is given by Eq. 3
- 336 (Liu et al., 2013):

337
$$MAC(\lambda) = \frac{\beta_{abs}(\lambda)}{C}$$
 (3)

- 338 where C is the concentration of the dissolved organic in a particular solvent (g m^{-3}). C for methanol and
- water soluble organics (C_{MSOC} and C_{WSOC} respectively) were calculated as:

341
$$C_{MSOC} = \frac{\text{(OC in original filter)} - \text{(OC in methanol extracted filter)}}{volume \ of \ methanol \ used \ for \ extraction}$$
(4a)

342 and,

340

344

343
$$C_{WSOC} = \frac{(\text{OC in original filter}) - (\text{OC in water extracted filter})}{volume \ of \ water \ used \ for \ extraction}$$
(4b)

- 345 C_{WSOC} was also directly measured from the aqueous filter extracts using a total organic carbon (TOC/TN)
- 346 analyzer (TOC-L, Shimadzu) to compare with the estimates obtained using Eq. 4b. Overall the two methods





yielded comparable C_{WSOC} values (R² = 0.98, Fig. S5,), so for consistency we have used the filter based C
 values for both MSOC and WSOC in calculating MAC. The imaginary part of the refractive index, k, was
 related to MAC at any given wavelength λ according to Jennings et al. (1979):

350
$$MAC(\lambda) = \frac{4\pi k(\lambda)}{\rho \lambda}$$
 (5)

where ρ is the density of the dissolved organic (g cm⁻³). For fresh, photochemically aged and dark aged emissions different mean density values were used for calculating k as mentioned in Table S4. For the RWC experiments, particle densities measured for fresh and PEAR-aged beech combustion exhaust particles from the same appliance (Mukherjee et al., 2024). were applied for the calculation of k. Specifically, density values of $1(\pm 0.1)$ g cm⁻³ and $1.6(\pm 0.1)$ g cm⁻³ were used for the primary and aged RWC exhaust particles, respectively.

Absorption Ångström exponent (AAE) of MSOC and WSOC were estimated between a pair of wavelengths λ_1 and λ_2 as the power law exponent of the ratio between the absorption coefficients at the two wavelengths (Moosmüller et al., 2009), such as:

361
$$AAE(\lambda 1, \lambda 2) = \frac{\ln\{\beta_{abs}(\lambda 1)/\beta_{abs}(\lambda 2)\}}{\ln(\lambda 2/\lambda 1)}$$
 (6)

For this study, AAE between wavelengths 300-550 nm were used to describe the optical behaviour of BrC emitted from different biomass sources. The wavelength dependence of the imaginary refractive index k is denoted as w (Saleh et al., 2014) which we derived for fresh and chamber samples using a similar power law relationship as Eq. 5 but involving k at two different wavelengths. In literature, w has also been estimated using AAE (Saleh et al., 2014, McClure et al., 2020) as they are related by:

$$367 \quad AAE \approx w + 1 \tag{7}$$

2.8 Emission Factor Calculation

Emission factors from the combustion experiments were calculated by the carbon mass balance method such

(Eq. 8; Yokelson et al., 1999)





371
$$EF_X = F_C \cdot 1000 \cdot \frac{ER_X}{\frac{\sum \Delta C}{\Delta CO}}$$
 (8)

- 372 where F_c is carbon fraction in the combusted sample and the summation $\sum \Delta C$ is the total carbon released
- 373 during the combustion. For savanna biomasses (SG and SW) $\Sigma\Delta C$ was estimated as (Vakkari et al., 2025):

374
$$\sum \Delta C = \Delta C O_2 + \Delta C O + \Delta C H_4 + \Delta O C + \Delta C H_5 + \sum \Delta C_{VOC}$$
 (9 a),

- 375 ΔCO₂, ΔCO and ΔCH₄ were their respective concentrations in ppm subtracted by background and synthetic
- 376 air concentration, ΔOC was measured by AMS, rBC was measured by SP2 and VOCs were measured by
- 377 VOCUS. For commercial peat (CP), boreal forest surface (BFS) and natural peatland (FIA, FIB, RUS and
- NOR) emissions, $\sum \Delta C$ weas estimated as:

379
$$\sum \Delta C = \Delta C O_2 + \Delta C O + \Delta C H_4 + \Delta O C + \Delta E C + \sum \Delta C_{VOC}$$
 (9 b),

- 380 For CP and BFS, CO₂, CO and CH₄ were measured using Picarro and non-methane VOCs (NMVOC) were
- 381 estimated from FTIR (Table S2). For natural peatland samples CO2, CO, CH4 and NMVOCs were all
- 382 measured by FTIR. OC and EC for all of these samples were estimated from OC-EC analyses of filters.
- 383 ER_x in Eq. 4 is the ratio of measured concentration in μg m⁻³ relative to the CO carbon concentration in
- 384 µgC m⁻³. ER_x was calculated by Eq. 5, where the CO concentration measured in ppm is converted to CO
- 385 carbon concentration in μgC m⁻³ using the following equation:

386
$$\Delta ER_X = \frac{X}{\frac{12.01 \, g/mol \times 101325 \, Pa}{8.31451 \, l/mol \cdot K \times (295.15 \, K + T)} x \Delta CO}$$
 (10)

- 387 Where X is the concentration of the measured parameter in μg m⁻³, ΔCO is the CO concentration in the
- 388 emission in ppm compared to background, T is measured temperature in the chamber in Kelvin (295.15 K or
- 389 22°C), 12.01 is the molecular weight of carbon (g mol⁻¹), 101325 standard atmospheric pressure in Pa,
- 390 8.31451 is gas constant in SI unit.

391 2.9 FT-ICR MS analyses:

- 392 Chemical compositions of the biomass burning emission samples collected on quartz filters were
- 393 characterized by means of ultrahigh-resolution mass spectrometry. All experiments were performed using a





394 12-T Bruker solariX XR Fourier transform ion cyclotron resonance mass spectrometer (FT-ICR MS) (Bruker 395 Daltonics GmbH, Bremen, Germany), equipped with a dynamically harmonized ICR cell (ParaCell®). The 396 mass spectrometer was coupled to an Apollo-II atmospheric pressure chemical ionization (APCI) source, 397 fitted with a direct insertion probe (DIP) accessory. This set-up enabled chemical characterization of the 398 filter samples directly with minimal sample preparation. Five layers of each quartz filter sample were packed 399 into a prebaked glass capillary (Hirschmann melting point tube) and inserted into the ion source vaporizer, 400 held at 370 °C. The capillary voltage was set to 4500 V and corona current to 4000 nA. Dry nitrogen was 401 used as the drying (3.5 Lmin⁻¹, 220 °C) and nebulizing (2.0 bar) gas. After an induction time of 10 s, the MS 402 data were recorded until the total ion current plateaued (i.e number of scans ranged from 15 to 35), indicating 403 that the entire aerosol sample was completely desorbed at the given temperature. 404 All DIP-APCI FT-ICR measurements were conducted in a positive ion mode. The generated ions were 405 accumulated in the hexapole ion trap and transferred to the ICR cell for trapping, excitation and detection. 406 The instrument control and data acquisition were performed by Bruker ftmsControl 2.1 software. For each 407 spectrum, a broadband frequency excitation and detection were carried out with 4 MWord time-domain 408 transients (transient time 1.1 s), which were full-sine apodized and zero-filled once to provide the final 8 409 MWord magnitude-mode data spanning m/z range of 100–2000. The time-of-flight and ion accumulation 410 time settings were 1.0 ms and 0.30 s, respectively. 411 The FT-ICR instrument was externally m/z-calibrated prior to the measurements using a polystyrene (PS) 412 standard covering a wide mass range and reaching accuracies generally below 1 ppm. The initial spectral 413 post-processing was done with Bruker DataAnalysis 5.1 software, including the internal re-calibration of the 414 m/z-axes with a custom-made mass list for organic aerosol samples. For the peak picking, a signal-to-noise 415 (S/N) ratio was set at ≥6. PetroOrg IS 18.0.3 software (Omics LLC, Tallahassee, FL, USA) was used for the 416 molecular formula assignments with the following constraints: double bond equivalent (DBE) 0-40; mass error ± 1.0 ppm; atomic formula $^{12}C_{1-100}{}^{1}H_{1-200}{}^{14}N_{1-4}{}^{16}O_{1-15}{}^{32}S_{1-4}$. The elemental composition boundaries for 417 418 the annotation were chosen based on careful manual inspection of spectra identifying the edges of the 419 observed chemical space. The time-resolved spectral information of the DIP experiment had been summed to 420 an average spectral read back for each measurement.





421 For data interpretation and visualization of the complex lists of attributed sum formulae, we used established 422 data grouping and fingerprint diagrams (Schneider et al., 2024a; 2024b). Visualization and pre-processing, 423 calculating molecular properties and diagnostic measures from the sum formulae were performed via 424 MATLAB (MATLAB R2023a, MathWorks Inc., MA). Characteristic molecular properties encompassed 425 double bond equivalents (DBE), aromaticity index (AI), saturation vapor pressure (C*) and average carbon 426 oxidation state (OS_C) frequently used in ultra-high resolution mass spectrometric studies of complex 427 environmental sample materials (Koch and Dittmar, 2006; Kroll et al., 2011; Li et al., 2016) 428 2.10: SP-AMS analyses: 429 This study employed a soot particle aerosol mass spectrometer (SP-AMS; Aerodyne Research Inc., Billerica, 430 MA, USA; Onasch et al., 2012) to analyze the concentration levels, mass spectral signatures, and size 431 distributions of non-refractory (organics, sulfate, nitrate, ammonium, and chloride) and refractory (e.g. 432 metals, rBC) components. The SP-AMS enhances the capabilities of the standard AMS by incorporating a 433 laser vaporizer, which enables the analysis of refractory aerosol components. While the instrument can 434 function using only the laser vaporizer, both the laser and tungsten vaporizers were used in this study to 435 ensure comprehensive detection of mentioned chemical species. Size-resolved measurements were obtained 436 using particle time-of-flight (PToF) mode, with the SP-AMS aerodynamic lens enabling detection of 437 particles ranging from roughly 50 nm to 1 µm. The instrument operated with a time resolution of 60 seconds, 438 with about half of the time measuring in mass spectrum mode and the other half in PToF mode. A calibration 439 of the SP-AMS based on particle mass was carried out using size-selected, dried particles of ammonium 440 nitrate and ammonium sulfate. This approach allowed for the determination of an effective nitrate response 441 factor, as well as the relative ionization efficiencies (RIEs) for ammonium (RIENH4) and sulfate (RIESO4), 442 by converting the instrument signals into nitrate-equivalent mass concentrations. The determined RIE value 443 for NH4 was 3.4 while the one for sulfate was 0.9. A default RIE value of 1.4 was used for organics. SP-444 AMS data processing was conducted using the AMS analysis tools SQUIRREL (version 1.63B) and PIKA 445 (version 1.23B) within Igor Pro 8 (Wavemetrics, Lake Oswego, OR).

446



448

449

450

451

452

453

454

455

456

457

458

459

460

461

462

463

464

465

466

467 468

469

470

471

472

473



3. Results

3.1 Emission factors of OC and EC in fresh emission

The emission factors of OC (EF_{OC}) and EC (EF_{EC}) were determined based on thermal-optical carbon analyses of filters collected from fresh exhaust aerosol (Fig. 2, Fig. S6). Generally, we observed higher EF_{OC} for smouldering combustions with low MCE, as expected. For EC however, the trend was reversed, with flaming combustion having higher MCE producing more EC per kg of fuel (Fig. S6). The combustion emissions in our experiments were OC rich, most likely due to the open setup of the burner, which resulted in lower combustion temperature compared to wood stove emissions, due to high air-to-fuel ratios and because there is no combustion chamber around the fire to retain the heat in the surroundings. However, there were significant variations in EFoc obtained from different combustion conditions and for different biomasses, ranging from 1.39-7.44 g kg⁻¹ for flaming dominated combustions and 6.12-89.9 g kg⁻¹ for smouldering dominated combustions. CP and SW samples had the largest EF_{OC} of 53.4(±29.0) g kg⁻¹ and 50.6(±29.8) g kg⁻¹ respectively, during the smouldering combustion phase. In contrast, full combustion of different natural peat samples yielded EF_{OC} in the range of 5.06-32.7 g kg⁻¹, with FIA (at depth of 30-60 cm) having the smallest (6.09±1.2 g kg⁻¹) and FIB (at depth of 30-60 cm) having the largest (29.8±2.92 g kg⁻¹) average EF_{OC} among peat samples. Interestingly, the average MCE values and EF_{OC} reported for field measurements of subtropical Indonesian peat fires (Stockwell et al., 2015; Jayarathne et al., 2018) and laboratory studies of North American (Black et al., 2016; Chakrabarty et al., 2016), West European (Iinuma et al., 2007) and South-east Asian peat fires (Christian et al., 2003; Iinuma et al., 2007) fell inside the range of our reported EF_{OC for} laboratory combustion of Finnish (boreal) and arctic peat samples. In our study, flaming and smouldering combustion of BFS samples had average EF_{OC} of 3.17(±0.77) g kg⁻¹ and 21.5(±13.8) g kg⁻¹ respectively, while previously reported EF_{OC} for North American boreal forest fires were in similar range of 5.9(±2.5) g kg⁻¹ (Andreae, 2019). Savanna wood and grass (SW and SG) samples burnt under flaming conditions in this study were estimated to have average EF_{OC} of 6.47(±0.98) g kg⁻¹ and $3.56(\pm 0.91)$ g kg⁻¹ respectively, which were somewhat higher in comparison to previously reported organic emission factor of 3.0(±1.5) g kg⁻¹ (Andreae, 2019) and 2.62(±1.24) g kg⁻¹ (Akagi et al., 2011) from high MCE savanna fires.





474 Emissions from savanna biomass had higher average EF_{EC} compared to the other biomasses, 475 with an average EF_{EC} of 3.03(±1.77) g kg⁻¹ and 0.94(±0.16) g kg⁻¹ from the smouldering emissions of the 476 woody (SW) and grassy (SG) fuels respectively. The carbonaceous fraction of flaming dominated emissions 477 from the woody savanna samples (MCE ~0.94±0.01) consisted of 12(±2) % of EC while savanna grass had 478 an EC content of $7.4(\pm 1.5)\%$ (MCE $\sim 0.96\pm 0.01$). Previously reported average EF_{EC} values for savanna and 479 grassland fires ranged from $0.37(\pm 0.20 \text{ g kg}^{-1})$ (Akagi et al., 2011) to $0.53(\pm 0.35)$ g kg⁻¹ (Andreae, 2019) 480 while Vakkari et al. (2018) reported EF_{EC} of 0.67 g kg⁻¹ for South African savanna grass burning. These 481 values fell in between our estimated EF_{EC} from flaming burn of savanna grass (0.27±0.01 g kg⁻¹) and wood 482 (0.72±0.17 g kg⁻¹). Full combustion (MCE 0.74-0.89) of the Finnish peat samples (FIA and FIB) collected at 483 the depth of 30-60 cm from the surface level and arctic permafrost peat samples from Svalbard (NOR) and 484 Russia (RUS) had the lowest measured average EF_{EC} (in the range of 0.02-0.13 g kg⁻¹), which matched well 485 with previously reported EF_{EC} from field and lab studies of subtropical Indonesian (Stockwell et al., 2015; 486 Christian et al., 2003) and laboratory replicates of North American peat fires (Black et al., 2016). Flaming 487 and smouldering combustions of CP had average EF_{EC} of 0.70(±0.65) g kg⁻¹ and 0.28(±0.14) which 488 resembled EF_{EC} reported from laboratory studies of Western European and South-East Asian peat fires 489 (Iinuma et al., 2007). Burning of the boreal forest surface sample (BFS) resulted in higher EC emissions than 490 any of the peat samples with an average EF_{EC} of $0.45(\pm0.16)$ g kg⁻¹ for high MCE (~0.94±0.01) combustion 491 and an average EF_{EC} of 0.11(±0.09) g kg⁻¹ for low MCE (~0.76±0.02) smouldering burns. For North 492 American boreal forest fires, Andreae (2019) reported EF_{EC} of 0.43(±0.21) g kg⁻¹ with the fire having an 493 average MCE of 0.89(±0.04), which resembles Finnish BFS EF_{EC} for flaming dominated burns. Thus, it 494 seems that our experiments with simulated surface fire conditions at comparably lower combustion 495 temperature typical for Eurasian wildfires yield similar EC emissions as reported for North American 496 wildfires that are commonly high temperature crown fires. 497 In comparison, for residential wood combustion (RWC) of North European beech wood logs 498 (Mukherjee et al., 2024) the respective average OC and EC emission factors were 0.64(±0.31) g kg⁻¹ and 499 0.28(±0.04) g kg⁻¹, respectively. Therefore, the OC emission factors for the open burning in the current study 500 were approximately 4-140 times higher for smouldering emissions and 2-13 times higher for flaming





emissions than our previous estimates of RWC emission. In comparison, we did not observe such a significant difference between the EC emission factors of RWC and flaming BB emissions. This implies that surface fires have the potential to be important sources of specifically organic pollutants and BrC in forest fire prone environments, whereas the BC emissions would not be particularly strong from these fires.

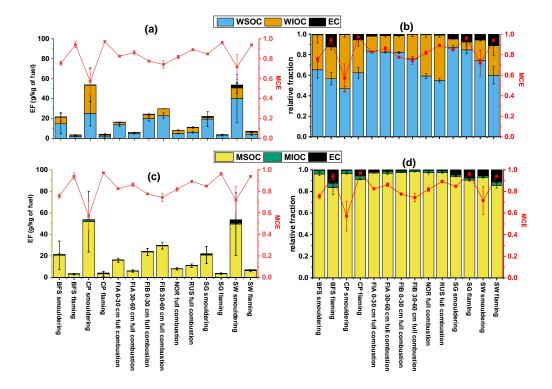


Figure 2. Emission factors of water-soluble (WSOC), methanol-soluble (MSOC), water-insoluble (WIOC), methanol-insoluble organic carbon (MIOC) and elemental carbon (EC) in absolute scale (a,c) and relative to total EF (b,d).

3.2 Chemical composition and solubility of fresh organic aerosol

Chemical characterization of the fresh emission samples from whole combustions of peat (FIA, FIB, RUS and NOR) and Finnish BFS have been previously reported by Schneider et al. (2024a) in which electrospray ionization (ESI) was utilized for the FT-ICR mass spectrometry on extracts, targeting the polar constituents. For this study, the filters containing specifically flaming and smouldering emissions of CP and BFS were analyzed directly from the filters by using 12-T DIP-APCI FTICR-MS to identify differences in the organic

https://doi.org/10.5194/egusphere-2025-2759 Preprint. Discussion started: 26 June 2025 © Author(s) 2025. CC BY 4.0 License.



515

516

517

518

519

520

521

522

523

524

525

526

527

528

529

530

531

532

533

534



matter compositions due to both fuel and combustion conditions. The advantage of the DIP-APCI technique used in this study is the ability to detect analytes with low solvent extraction recoveries due to minimal sample preparation required (Rüger et al., 2021). Additionally, APCI was able to address a wide chemical space covering polar up to apolar analytes. Therefore, inspite of the lower mass loadings on the filters for specific combustion phases compared to full biomass combustions as reported in Schneider et al. (2024a), we could assign up to 2000-4000 monoisotopic elemental compositions. Overall, CHO, CHNO and CH compound classes were the most abundant in the fresh BB emissions of CP and BFS. The low temperature smouldering combustions have been shown to emit mostly direct thermal degradation products from biomass pyrolysis (Chakrabarty et al., 2016) compared to flaming combustion (Engling et al., 2006, Popovicheva et al., 2019), with similar chemical composition and molecular structures to that of the fuel (Kourtchev et al., 2011). Similar to the smouldering dominated peat burning emissions reported in Schneider et al. (2024a), we also observed that the CP smouldering emissions were chemically most diverse with the highest number of sum formulae unique to this burning condition (in total 774), thus reflecting the complex inherent compositional variability of the peat samples (Figure 3). CP smouldering emissions also had clearly higher CHN and CHNO fractions than all the other biomasses and combustion conditions. This observation can be attributed to the fact that the CP samples contained only below-surface peat that have decomposed for longer time periods and experienced more microbial activity than the BFS samples, leading to higher N containing species. Flaming combustion of CP emitted the second highest number of unique sum formulae (in total 297) but had much lower CHN class content compared to smouldering conditions, suggesting a considerable effect of the burning condition / MCE on the POA chemical composition (Figure 3).





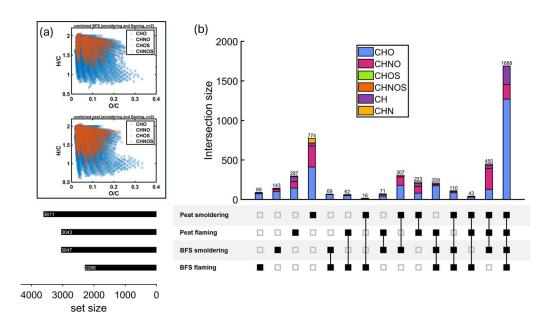


Figure 3: (a) Van-Krevelen diagrams of oxygen-containing compounds and (b) upset plot intersections (combined CP and BFS) with compound class indicated by colour. Samples were analyzed by positive-ion DIP-APCI FT-ICR mass spectrometry. Upset plot of four organic aerosol datasets with the number of measured molecular formulae in the whole dataset (bottom left) and the individual intersections (top right) indicated by color (CHO-light blue, CHOS-green, CH-purple, CHNO-magenta, CHNOS-orange and CHN-yellow)

On the other hand, the BFS smouldering and flaming emissions exhibited chemically similar compounds, with nearly 1900 identified molecular formulae shared among all the analyzed BFS samples. Almost none of the molecular formulae were unique to BFS smouldering or flaming samples, as the variability among replicates themselves was high. This indicates that although different combustion conditions of BFS strongly influence the OC emission factor, it does not lead to prominent chemical differences in POA. Similar to CP, BFS emissions were also dominated by CHO, CHNO and CH classes, although a much lower fraction of CHN was present in the BFS smouldering emission compared to CP. Furthermore, a more detailed inspection of the identified formulae of the nitrogen-containing molecules in the fresh CP and BFS emissions reveals that they mostly belonged to the CHNO class, contained one nitrogen substitution, and consisted of both aliphatic and aromatic nitro-organic compounds (Figure 4). Specifically, nitroaromatics were more





abundant in the peat samples, which is relevant, as nitroaromatics are known to be prominent BrC chromophores absorbing light in the wavelength range of 360-600 nm (Fleming et al., 2020).

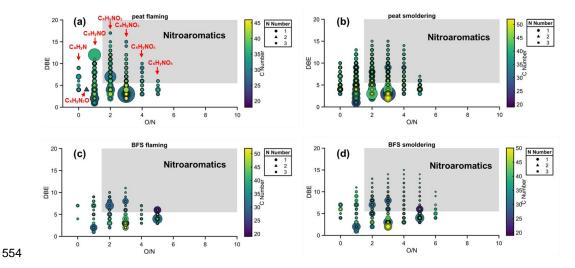


Figure 4: Detailed chemical characterization of CHN and CHNO compounds in (a) CP flaming, (b) CP smouldering, (c) BFS flaming and (d) BFS smouldering fresh emissions. The x-axis shows O:N ratio and y-axis corresponds to double-bond equivalence (DBE). Nitroaromatic compounds fall into the shaded (grey) area in the figures.

Due to their different chemical compositions, OC from various fresh BB emissions exhibited variable solubility in water and methanol (Fig. 2, Fig. S11). While methanol extracted almost all the OC (~95%) from the filter irrespective of fuel or combustion type, the water-soluble fraction of OC (WSOC) exhibited fuel dependent behaviour. For example, both FIA and FIB emissions exhibited higher WSOC fractions (76-83%) in the total organic carbon (TOC) compared to arctic permafrost peat samples NOR (~59% of TOC) and RUS (~55% of TOC). This has been previously elaborated by Schneider et al. (2024a), who found that in comparison to FIA and FIB samples, NOR and RUS peat combustion emissions were constituted by less oxidized primary organic carbon (POC), which explains the diminished solubility in a polar solvent like water (Budisulistiorini et al., 2017). Among the biomass samples used in this study, SG showed the highest WSOC fractions for both flaming (~92% of TOC) and smouldering (~91% of TOC) combustion (Fig. 2c-d), suggesting abundance of more oxidized POC in these emissions, while smouldering burning of CP consisted of the smallest WSOC fraction (~46%). These observations point towards the presence of non-polar organic







moieties, which are soluble in methanol but not in water, as previously reported in the literature (Lin et al., 2017).

Due to the variation in chemical composition and solubility of the fresh BB emissions, we observed

573

574

575

571

572

3.3 Optical properties of Fresh organic aerosol:

576 substantial diversity in the optical properties of the freshly emitted organic particles. Since MSOC 577 corresponded to around 95% of the total OC in our fresh BB emissions, we can use MSOC as a proxy for 578 BBOA in our study. The absorption angstrom exponent (AAE₃₀₀₋₅₅₀, measured in the range of 300-550 nm) of 579 the particles sampled from the fresh emission for different fuels ranged between 4.4-5.3 and 4.7-6.2 for 580 WSOC and MSOC, respectively. These values fall in the ranges of previously reported AAE for BB emitted 581 as well as urban WSOC and MSOC (Cao et al., 2021; Fan et al., 2018; Yan et al., 2015; Mukherjee et al., 582 2020). In general, for all samples, AAE_{MSOC} was found to be marginally higher than the respective AAE_{WSOC}. 583 The largest variability in AAE_{MSOC} was observed among BFS smouldering (5.5-6.2) and flaming (5.3-6.0) 584 samples, which was likely a result of the difference in combustion and heterogeneous vegetation distribution 585 in the burnt BFS samples. The Svalbard peat (NOR) emission displayed AAE_{WSOC} in the range of 4.6-5.2, 586 while its AAE_{MSOC} was constrained in the range of 4.9-5.2. In comparison to open BB, fresh RWC emissions 587 having high soot contents (Mukherjee et al., 2024; wood stove 1 in Figure S7) exhibited much lower AAE 588 for both WSOC and MSOC (2.2-2.4), while the wood combustions from the previous campaign (Ihalainen et 589 al., 2019a; wood stove 2 in Fig. S7) displayed larger AAE_{WSOC} (5.8-6.8) and AAE_{MSOC} (5-5.6). The lower 590 AAE values of RWC emissions indicates that BrC from high EC/OC emissions absorb light throughout the 591 measured spectral range, as shown earlier by Saleh et al. (2018). 592 The MAC values obtained from UV-vis spectroscopy at 365 nm for fresh BB emitted MSOC (MAC_{365 MSOC}) 593 were constrained between 0.46-1.48 m² g⁻¹ for the experiments. In comparison, MAC_{WSOC} was found to be in 594 the range of 0.51-1.78 m² g⁻¹. These MAC₃₆₅ values fall within the same range as observed for BBOA in 595 previous literature (Park and Yu, 2016; Huo et al., 2018; Moschos et al., 2018; Cao et al., 2021). Among 596 open BB experiments, the lowest MAC365 MSOC were generally observed for fresh emissions from BFS





smouldering combustions, while flaming combustion of CP and SW were estimated to have the highest MAC_{365_MSOC} (Table S4). The MAC_{365_MSOC} for smouldering SG and SW emissions were in a similar range to the MAC_{365_MSOC} values compared to smouldering emissions (Fig. 5a). In addition, MAC values for high temperature wood log combustion in the modern European stove were significantly higher than for open BB. Fresh RWC emissions had MAC_{365_MSOC} values in the range of 3.33-16.4 m² g⁻¹, while the MAC_{365_WSOC} values ranged from 0.32-4.96 m² g⁻¹. The correlation between the EC/OC ratios obtained for different experiments to the corresponding MAC_{MSOC} also suggests that EC rich emissions contribute to stronger BrC light absorption (Fig. 5a). Formation of BrC internally mixed with soot particles in high temperature BB emissions has been shown to contribute to enhanced light absorption in past studies, due to lensing effect (Jacobson et al., 2001; Liu et al., 2015; Liu et al., 2017; Zhang et al., 2025), which supports our observation.

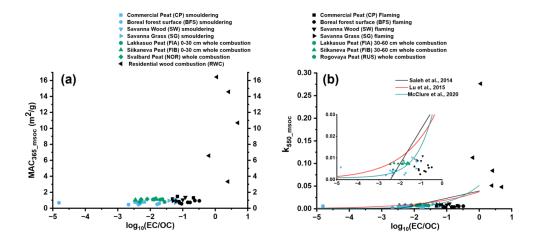


Figure 5: Relationships between MAC_{365_MSOC} (a) and k_{550_MSOC} (b) with EC/OC of open BB and RWC emissions. We observe increasing MAC and k for high temperature combustions with higher EC/OC ratio

The imaginary refractive index measured at the middle of the visible light spectrum at 550 nm (k₅₅₀) for the BB MSOC varied across orders of magnitude and ranged between 0.002-0.011(Fig. 5b, Table S4) in our experiment. Similar to MAC, the smouldering emissions exhibited lower k_{550_msoc} than the flaming dominated

burns. As shown in previous studies (Saleh et al., 2018; Saleh et al., 2020) there seem to exist a continuum between the ratio of EC/OC in the fresh BB emission to the BrC light absorption, as we again observed





enhanced k_{550_msoc} for EC rich wood stove emissions (fig. 5b). Most of the fresh BB MSOC fell in the weak BrC regime in the "k-w" space (Fig. 6a), proposed by Saleh et al. (2018), while some of the wood stove combustion generated particles, in contrast, were in the strong BrC domain. These results fall in line with previous observations of high temperature (and high MCE) biomass combustions generating "darker BrC", which exhibit much stronger light absorption compared to lower temperature open BB emissions (Saleh et al., 2018). The data points in k-w space obtained in this study matches reasonably well with previous literature, as shown in Figure 6a.

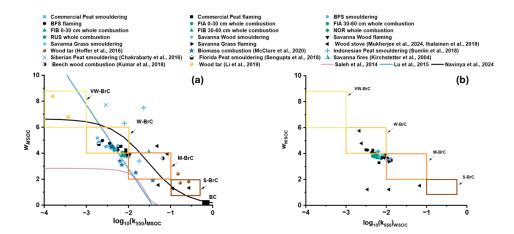


Figure 6: Relationship between w and k₅₅₀ for (a) MSOC and (b) WSOC in fresh emissions from smouldering (light blue points), flaming (black points), full combustion (green points) of open BB performed in this study. Rectangles denote the different light absorbing BrC classes. Several data points from previous literatures (Hoffer et al., 2016; McClure et al., 2020; Sumlin et al., 2018; Chakrabarty et al., 2016; Sengupta et al., 2018; Kirchstetter et al., 2004; Kumar et al., 2018; Li et al., 2019; Saleh et al., 2014; Lu et al., 2015; Navinya et al., 2024) have been added in (a) for reference.

3.4 Particle size distributions and morphologies of chamber diluted primary emissions

Particle size distribution, morphology and effective density were measured for chamber diluted primary emissions. Smouldering combustion of BB generally emitted more particles on average when compared to flaming combustion (Fig. S8). Overall, there was little variability in the particle size distributions for flaming

https://doi.org/10.5194/egusphere-2025-2759 Preprint. Discussion started: 26 June 2025 © Author(s) 2025. CC BY 4.0 License.



635

636

637

638

639

640

641

642

643

644

645

646

647

648

649

650

651

652

653

654

655

656

657

658

659

660

661



combustion experiments, irrespective of the biomass type. The average particle geometric mean diameters (GMD) ranged between 48 and 85 nm (Table 1). However, we observed clear variation in the emitted particle size distribution among the smouldering combustions, likely due to the unique combustion behaviour of individual samples with varying distributions of different types of biomass, such as surface vegetation, litter and woody branches. Smouldering combustion of BFS gave rise to distinct bimodal size distributions with the lower mode having a GMD of 30-40 nm, and the larger mode peaking around 100-175 nm. Some replicates of smouldering emissions from CP and SW burning also exhibited bimodal size distribution. The effective densities of primary particles inside the chamber varied between experimental replicates (Fig S9), which can again be explained by the variability in the combustion and emissions between experiments. The effective densities were largely independent of the particle diameter for all fuel type and combustion conditions (Fig. S9), unlike soot-rich RWC emissions that exhibited size-dependent behaviour in our previous work (Leskinen et al., 2014; Mukherjee et al., 2024). Due to the size-independent behaviour, we averaged over all experimentally obtained density values and estimated average particle densities for each BB emissions (Table S4). While CP and BFS combustion emitted particles had average densities of 1.1 g cm⁻³ and 1.20(±0.05) g cm⁻³ for both smouldering and flaming dominated combustions, SW and SG emitted particles were denser with average densities of 1.4 g cm⁻³ and 1.65(±0.05) g cm⁻³ for smouldering combustion respectively. For flaming combustions, SW emitted primary particles had an average density of $1.45(\pm 0.05)$ g cm⁻³ and SG particle density was 1.75(±0.05) g cm⁻³. Little to no size-dependency for particle density was observed in our experiments suggesting near-spherical particle morphology with mobility exponents close to 3 (Leskinen et al., 2023; Corbin et al., 2023). SEM images of chamber diluted primary emissions (Fig. S10) support these results, since mostly round organic particles were observed from the collected grids. These findings agree with the measured chemical compositions that indicated that freshly emitted particles consisted mostly of POC and very little EC, leading to formation of particles with a spherical morphology, so-called tarballs. Tarballs have been previously observed in BB emissions (Chakrabarty et al., 2010; China et al., 2013; Hoffer et al., 2016; Adachi et al., 2019) and atmospheric dilution and aging have been shown to aid the formation of spherical viscous tarball BrC (Hennigan et al., 2011; Sedlacek et al., 2018). In chamber diluted CP and BFS emissions, we observed mostly tarballs (Fig. S10a-d) but SG and SW emissions (Fig. S10e-h)

https://doi.org/10.5194/egusphere-2025-2759 Preprint. Discussion started: 26 June 2025 © Author(s) 2025. CC BY 4.0 License.





also had soot agglomerates that were partially coated or embedded with organics, as previously reported in China et al. (2013). Notably, the morphology of fresh particles emitted from open BB was very different to those emitted from a wood stove (Mukherjee et al., 2024), where the high temperature combustion formed mostly chain-like fractal soot agglomerate structures which were mostly bare or with some organic inclusions (Fig. S10i; China et al., 2013).

3.5 Effect of chamber dilution on the properties of fresh emission aerosols

The relative fractions of OC1, OC2, OC3, OC4, Pyrol C and EC in fresh emissions differed before and after dilution in the chamber (Fig.7; Table S3), highlighting the effect of dilution on the overall chemical composition of BB emissions. The relative fraction of the intermediate volatility (IVOC) and semi-volatile organics (SVOC), namely OC1 and OC2 obtained from IMPROVE-A protocol (Ma et al., 2016) were lower in the diluted chamber samples than in the fresh emissions, while the low volatile fractions from OC3 to PC increased (Fig. 7). We might have over-estimated the OC1 fraction in fresh emission due to gas phase VOC adsorption on the filter surface causing positive artifact (Kirchstetter et al., 2001). However, the significant increase in low volatile OC fractions (OC3, OC4 and PC) in chamber samples indicate dilution related evaporative loss of the volatile OC fractions in the chamber due to partitioning between gas and particle phase (Calderon-Arrieta et al., 2024).





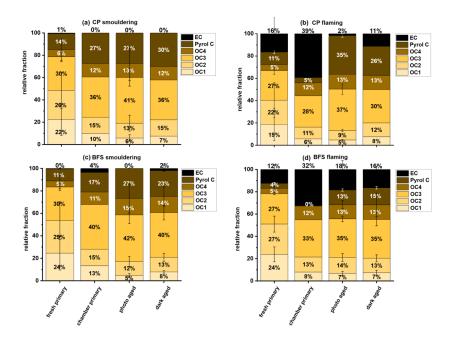


Figure 7: The relative abundance of different OC fractions and EC measured in BB emissions from (a) fresh emission, (b) fresh emission after dilution in chamber, (c) photochemically and (d) dark aged emission in the chamber. Error bar indicates the variability among experimental replicates

The partitioning of OC1 and OC2 fractions between gaseous and condensed phases is largely influenced by the prevailing concentrations in the collected aerosol. Thus, a clear trend is seen between the share of low volatile OC fractions (OC3+OC4+PC) to the total OC and the collected aerosol OC concentration (Fig. 8). The dilution and consequent evaporation of the most volatile OC also influences the solubility of the POC of the fresh emission. Methanol extraction efficiency significantly decreased for the more diluted POC in the chamber (Fig. S11b). This is in line with the change in volatility as the low volatile OC fraction, including tarball BrC, is generally less soluble in solvents (Chakrabarty et al., 2023; Saleh et al., 2020).



691

692

693

694 695

696

697

698

699

700

701

702

703

704

705

706 707

708

709



8000

12000

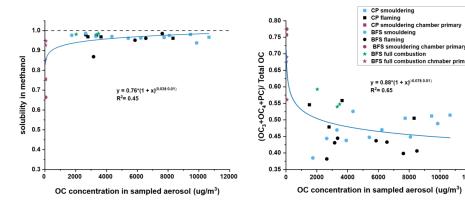


Figure 8: Effect of OC concentration on the partitioning of the OC fractions in BB emissions. Higher dilution in the chamber resulting in lower OC concentration result into larger fraction of low volatile OC fractions and lower solubility in methanol

The increment in the low volatile OC fractions in chamber diluted primary emissions could also be seen from the abundance of spherical tarballs in the SEM images (Fig. S15). We postulate, based on indirect evidence and previous knowledge, that the fresh BB emission collected on the filters probably had poorly formed tarballs (consisting of higher OC1 and OC2 fractions) and higher methanol extractable OC. After the dilution related change in volatility distribution of the OC in the chamber (Calderon-Arrieta et al., 2024), methanol insoluble, highly viscous and spherical tarballs were formed in the chamber (Heninghan et al., 2011; Sedlacek et al., 2018; Adachi and Buseck, 2011). Interestingly, we observed a slight increase in the solubility of WSOC for chamber primary samples (Fig. S11a). This might be the effect of low OC amount filters collecting chamber diluted samples, leading to higher water to OC ratio during the extraction. Thus, the volume of water used for extracting chamber primary filter punches allowed the dissolution of sparingly water-soluble organics.

The change in particle volatility and solubility due to dilution in the chamber did not significantly affect the light absorption wavelength dependency of MSOC and WSOC. The AAE_{MSOC} and AAE_{WSOC} of chamber diluted samples ranged from 5.5-6.1 and 5-5.9, respectively. At the same time, the AAE_{MSOC} and AAE_{WSOC}





for the corresponding freshly emitted particles were 5.3-5.6 and 4.6-5.3, respectively. However, we observed
a 17% decrease in MAC_{365_MSOC} (Fig. S12) and a 25% decrease in MAC_{365_WSOC} (Fig. S13) in the chamber
primary samples compared to fresh emissions for BFS full combustion samples. This suggests that the
fraction of OC extracted by water and methanol in chamber diluted primary samples had smaller mass
absorption efficiency compared to those extracted from the fresh emissions. This can again be explained by
the formation of non-soluble dark BrC through the phenomenon termed as "darkening by volatilization" as
the low volatile fraction consists of stronger chromophores (Calderon-Arrieta et al., 2024).

3.6. Effects of simulated atmospheric aging on properties of particulate organic

719 matter

3.6.1 Effects of aging on volatility and solubility of OC

The relative OC fractions of chamber diluted primary particles and aged particles seemed to be similar (Fig. 7), suggesting that when it comes to the relative distribution of the OC volatility in BB emissions, the effect of dilution in the environmental chamber outweighed the impact of photo and dark oxidative aging we achieved in our experiments. After oxidative aging there were, however, further increments of the pyrolized carbon (PC), which is the lowest volatility organic fraction. Oxidative aging is known to increase the oxidation state and decrease the volatility of aged particles, making them more insoluble in organic solvents (Saleh et al., 2020). Expectedly, we observed that both photochemical and dark oxidative aging decreased the fraction of MSOC significantly (Figure S11b). On the other hand, the more oxygenated aged OC exhibited slightly higher WSOC compared to POC in fresh emissions, and we observed a medium correlation (R = 0.5) between water solubility and the atomic O:C ratio obtained from SP-AMS (Fig. S14b). The only exception to this were the smouldering emissions of CP and BFS, which did not exhibit any significant change in water solubility after dark or photochemical aging. This suggests that the chamber diluted POA emitted from smouldering burns are more resistant to photochemical or dark oxidation, inadvertently hinting towards the highly viscous tarball BrC. Tarballs are known to be resistant to chemical oxidation (Chakrabarty et al.,





2023) and we also observed the formation of more stable dark tarballs, especially in smouldering emissions,

due to oxidative aging in the chamber (Fig. S15).

3.6.2 Effects of aging on organic matter density

Oxidative aging, both in photochemical and high NO_x dark conditions, led to a marginal increment in particle densities for BFS emissions. For BFS smouldering emission, the effective density after photochemical aging increased to $1.30\pm0.05~g~cm^{-3}$ while no significant change was observed between primary and dark aged particle densities. For flaming dominated combustion, the particle densities increased under both photochemical ($1.30\pm0.09~g~cm^{-3}$) and dark aging conditions ($1.30\pm0.07~g~cm^{-3}$). For CP, the effective density of high NO_x dark aged particulate emissions remained unaltered at $1.1~g~cm^{-3}$, while photochemically aged emissions exhibited higher density. For SW emissions, both photochemical aging and low NO_x dark aging appeared to have a negligible impact on overall particle effective densities (Table S4). In contrast, particle effective densities for flaming and smouldering combustion of SG emissions seemed to be lower after undergoing photochemical and dark aging (Table S4).

3.6.3 Effects of aging on organic matter chemical composition

Due to low OC loading on the filters collected from the chamber, we were only able to assign roughly 120-600 unique elemental formulae of the most abundant chemical compounds from FT-ICR MS analyses of the photo and dark aged samples of CP and BFS, while signals arising from other compounds were below the detection threshold (S/N ≥6) (Fig. S16, S17). Therefore, we were unable to perform a one-to-one comparison of the chemical compositions of the fresh emission with the chamber-aged samples. However, we could conclude that CH and CHO were the most abundant compound classes in the chamber diluted primary and aged samples for both CP and BFS. We obtained elemental ratios (O:C, H:C and N:C) of the chamber diluted primary and aged samples from the SP-AMS measurement to characterize the variability in the bulk composition of the OC. The resulting Van-Krevelen plots (Fig. S18) showed that the chamber diluted primary emission had H:C values close to 2.0, while the O:C and N:C values ranged between 0.10-0.25 and 0.013-0.027, respectively. We observed an increment in the O:C ratios in the chamber aged emission while





761 the H:C ratio decreased, as in some previous studies (Lambe et al., 2011). On the other hand, after high NO_x 762 dark aging, the overall N:C ratio did not display a similar increase, probably due to the fast degradation of 763 the nitroaromatics formed inside the chamber at the time of filter collection at the end of the experiments. 764 3.6.4 Effects of aging on optical properties 765 Photochemical aging increased AAE and the wavelength dependency of k (w) of the BB emissions for both 766 MSOC and WSOC. The light absorption shifted towards smaller wavelengths (fig. S19) while the k at 550 767 nm either remained unchanged or decreased (Fig. 9). wwsoc and wmsoc varied between 3.3-3.7 and 4.3-4.5 768 respectively for fresh emission of CP, while it increased to 4.0-5.1 and 4.0-6.4 after photochemical aging. 769 The largest increase in w_{MSOC} was observed for flaming combustion of SG, where w_{MSOC} increased from 3.9 770 to 6.3, while k_{550 MSOC} decreased an order of magnitude. All the photochemically aged WSOC and MSOC 771 samples in this study lied in the w-BrC to vw-BrC region of the k-w space. This behaviour is in line with the 772 effects of photobleaching and photolysis during OH exposure in the presence of UV lights. Increasing 773 photooxidation has been shown to cause fragmentation reactions after functionalization (Kroll et al., 2015; 774 Saleh et al., 2020). OH · has been shown to cleave polyaromatic chains and give rise to short unsaturated 775 chemical moieties that absorb light at the UV range of the spectrum. On the other hand, photochemical 776 aging of RWC emissions in oxidation flow reactor either decreased (for samples from Ihalainen et al., 2019a) 777 or increased (Mukherjee et al., 2024) the k_{550 msoc}, suggesting that chemical composition of the precursor 778 organic molecules and the reaction pathways are consequential to secondary BrC optical properties (Lambe 779 et al., 2013; Sumlin et al., 2017; Hems et al., 2020). 780 781 The effect of dark aging on the optical properties was more non-trivial in our study. We noted that for 782 flaming dominated emissions, the NO_x dominated dark aging led to higher k₅₅₀ values and decreasing w 783 values (fig. 9) in accordance with Saleh (2020). This means an increase in light absorption towards the 784 visible wavelength range, which was also seen in the absorption spectra (fig. S19). On the other hand, dark 785 aging seemed to have very minor effect on the smouldering dominated emissions. One explanation for this 786 observation could be the prevalence of tarballs in the smouldering dominated emissions of both peat and 787 other biomass samples, which have been shown to be quite resistant to oxidative aging (Chakrabarty et al.,





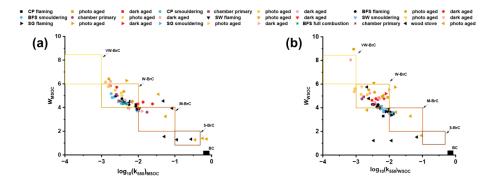
2023). Additionally, nitroaromatics are reactive, and certain fractions of them may have degraded at the end of the chamber experiments or during filter collection from the chamber, making it difficult to distinguish the effects on optical properties.

791

788

789

790



792

793

794

795

796

797

798

Figure 9: k-w space for all experimental data included in our study. Black, blue and green colours denote fresh emissions from flaming, smouldering and full combustion respectively. Purple dots denote primary emission in chamber without any aging (chamber primary). Dark yellow and red points denote photochemical and dark aging of flaming dominated emissions respectively, while light yellow and red dots represent respective photochemical and dark aging of smouldering dominated emissions.

799 emission 800 correspo 801 emission 802 suggest 803 absorpti

WSOC light absorption in "k-w space" (fig. 9b) suggests that the water soluble BrC in fresh and aged emissions of RWC had lower k₅₅₀ values and therefore less strongly absorbing chromophores than the corresponding MSOC samples. Certain dark aged samples, especially those for flaming BFS and SG emissions, also seemed to contain stronger chromophores in MSOC than in WSOC. These observations suggest that less polar organics, which are soluble in methanol but not in water, contribute to higher light absorption in these BB emissions. In addition, it should be noted that MSOC light absorption in the aged emissions might be underestimated, because fractions of the aged organics were non-soluble (Fig. S12b) and might have contained even stronger chromophores. In future, online measurements of OA absorption at different wavelengths is needed to confirm the observed effects of photochemical and dark aging.

807 808

804

805

806

4. Conclusions:





In this work, we estimated OC and EC emission factors and organic aerosol optical and chemical properties for different Eurasian open BB emissions, separately for flaming and smouldering dominated combustion. These characteristics were compared with two other major source-specific BB emissions; residential wood combustion and African savannah biomass burning. Open BB particulate emissions are generally dominated by OC and specifically smouldering conditions emit higher OC than flaming combustion, as expected. Open BB OC emission factors ranged from 1.39 to 89.9 g kg⁻¹ fuel.

Fraction of WSOC varied in the emissions from different biomasses, whereas nearly all of the emitted fresh OA was methanol soluble (>92%). Therefore, we used the optical properties of MSOC as a proxy for bulk BrC optical properties. The imaginary refractive index at 550 nm for MSOC (k_{550_MSOC}) of the fresh organic aerosols varied between 0.002 and 0.011, and fell into the category of weakly absorbing BrC, as classified by Saleh (2020). The MAC_{365_MSOC} ranged between 0.46 and 1.48 m² g⁻¹ and was observed to follow a continuum with respect to aerosol EC/OC-ratio. Consequently, flaming emissions exhibited higher MAC_{MSOC} (can be also called MAC_{OA}) than smouldering emissions. In addition, the biomass-type influenced light-absorption of OA, with peat emissions showing the highest MAC_{OA}, most likely due to their high abundance of nitroaromatic compounds. AAE_{MSOC} in the wavelength of 300-550 nm ranged between 4.2-6.2, indicating that the light absorption was strongly dominated by BrC chromophores that absorb at shorter wavelengths.

Further characterization of the BB emissions was carried out using an environmental chamber to simulate the effects of atmospheric dilution and oxidative aging on aerosol properties. Irrespective of biomass type, smouldering combustion generated higher particle number concentrations than flaming dominated burns. Tarball morphologies of variable sizes were observed for all open BB emissions and in all studied conditions. OC1 and OC2 fractions, that are the most volatile OC fractions and overlap with SVOC and IVOC, decreased in the chamber compared to fresh emissions, due to particle-to-gas partitioning in the chamber. This dilution induced change of OA volatility distribution resulted in higher fractions of OC3, OC4 and PC (SVOC, LVOC and ELVOC) and potentially formed stronger BrC chromophores (Calderon-Arrierta et al., 2024) in the chamber primary samples. However, we observed a slight decrease in MAC_{MSOC} for





wavelengths higher than 365 nm. This contrasting finding is likely because our solvent extraction method cannot resolve the lowest volatility fraction of OA in the chamber samples.

After photochemical and dark oxidation, the O:C ratio of the particles increased and resulted in increasing ELVOC fractions (PC in particular), making it more insoluble in methanol. Dark aged CP and BFS smouldering emissions in particular had the lowest methanol solubility, probably due to the high abundance of tarballs with high viscosity OA (Chakrabarty et al., 2023). On the other hand, WSOC fraction moderately increased after aging, likely due to the observed higher oxygenation and consequent polarization of the compounds. For the dark-aged samples, absorption increased for all wavelengths, suggesting the formation of stronger light-absorbing oxygenated compounds and/or nitroaromatics. For photochemically aged samples, MAC₃₆₅ increased but visible wavelength absorption, i.e k₅₅₀ decreased, probably due to photobleaching and breaking down of BrC chromophores. In future, the OA offline optical characterization should be accompanied by online aerosol optical measurements, to estimate light-absorption of non-soluble OA.

Overall, our results highlight that boreal forest surface fires as well as boreal and arctic peat fires are potentially important sources of BrC into the atmosphere. Further, we show that atmospheric dilution and oxidative aging influence BrC properties. This dynamic property of BrC should be considered in global climate models to correctly estimate direct radiative forcing of biomass burning emissions.

Data availability:

Essential data used in this study are available at FAIR-aligned data repository Zenodo via https://doi.org/10.5281/zenodo.15647186 with Creative Commons Attribution 4.0 International license (Mukherjee et al., 2025). Detailed mass spectrometry data are available upon request from the corresponding authors.

Author contribution:





860 VV, AnV, OS, AH, PYP, MI, KK and AB contributed in designing the study as well as supervising the whole 861 experimental campaign. KK and MR arranged for the arctic-boreal biomasses, whereas KJ, SJS, PGVZ and 862 VV collected, sorted and transported savanna biomasses to the study site in Finland. Measurements were 863 performed by AM, MaS, AH, MI, PYP, LMFB, DL, TuK, LV, AB, MuS and VV. Offline filter analyses, 864 including solvent extraction and thermal-optical analyses were performed by AM and VL, with supervisions 865 from NK. SEM images were captured by HK. FT- ICR MS analyses of filter samples and subsequent data 866 analyses and plotting were done by CPR, TiK, VHN and JJ. Other data analyses were performed by AM, 867 MaS, TuK, AH, LB and LV. The manuscript was prepared by AM with help from AH, OS, MR, KK, MaS, 868 LB, VN, TK, CR, JJ, HT and AkV. Fundings for this work were acquired by OS, AkV, AnV, VV and HT. 869 **Acknowledgements:** 870 The authors would like to thank adj. prof. Minna Väliranta (University of Helsinki), who kindly delivered 871 Arctic and boreal peat samples for this work by within the scope of an Arctic Avenue project. We would also 872 like to acknowledge Dr. Niko Kinnunen (Department of Environmental and Biological Sciences, University 873 of Eastern Finland) for his help regarding the TOC analyses. 874 **Financial support:** 875 This work was supported by the Research Council of Finland via the project "Black and Brown Carbon in 876 the Atmosphere and the Cryosphere" (BBrCAC) (decision number 341271), and projects 341597, 355871 877 and 343359 as well as Jane and Aatos Erkko Foundation project "Climate and air quality impacts of boreal 878 forest fires" (BoFF). The authors also gratefully acknowledge Research Council of Finland Flagship 879 fundings (grant no. 337550, 337552) and fundings from the European Commission under the Horizon 2020-880 Research and Innovation Framework Programme, H2020-INFRAIA-2020-1, Grant Agreement 881 number:101008004. A.M acknowledges the LUMETO Doctoral Fellowship provided by the University of 882 Eastern Finland. The mass spectrometry facility is supported by Biocenter Kuopio, Instruct Center Finland 883 (FINStruct) and Research Council of Finland (FIRI funding).





References:

- Adachi, K., & Buseck, P. R. (2011). Atmospheric tar balls from biomass burning in Mexico. *Journal of Geophysical Research*, *116*(D5), D05204. https://doi.org/10.1029/2010JD015102
- Adachi, K., Sedlacek, A. J., Kleinman, L., Springston, S. R., Wang, J., Chand, D., Hubbe, J. M.,
 Shilling, J. E., Onasch, T. B., Kinase, T., Sakata, K., Takahashi, Y., & Buseck, P. R. (2019).
 Spherical tarball particles form through rapid chemical and physical changes of organic matter
 in biomass-burning smoke. *Proceedings of the National Academy of Sciences of the United*
- 892 States of America, 116(39), 19336–19341. https://doi.org/10.1073/pnas.1900129116
- Adler, G., Wagner, N. L., Lamb, K. D., Manfred, K. M., Schwarz, J. P., Franchin, A., Middlebrook, A. M., Washenfelder, R. A., Womack, C. C., Yokelson, R. J., & Murphy, D. M. (2019). Evidence in biomass burning smoke for a light-absorbing aerosol with properties intermediate between brown and black carbon. *Aerosol Science and Technology*, *53*(9), 976–989. https://doi.org/10.1080/02786826.2019.1617832
- Akagi, S. K., Yokelson, R. J., Wiedinmyer, C., Alvarado, M. J., Reid, J. S., Karl, T., Crounse, J. D.,

 & Wennberg, P. O. (2011). Emission factors for open and domestic biomass burning for use in
 atmospheric models. *Atmospheric Chemistry and Physics*, *11*(9), 4039–4072.

 https://doi.org/10.5194/acp-11-4039-2011
- Andreae, M. O. (2019). Emission of trace gases and aerosols from biomass burning An updated assessment. *Atmospheric Chemistry and Physics*, *19*(13), 8523–8546. https://doi.org/10.5194/acp-19-8523-2019
- Atwi, K., Cheng, Z., El Hajj, O., Perrie, C., & Saleh, R. (2022). A dominant contribution to light
 absorption by methanol-insoluble brown carbon produced in the combustion of biomass fuels
 typically consumed in wildland fires in the United States. *Environmental Science:* Atmospheres, 2(2), 182–191. https://doi.org/10.1039/D1EA00065A
- Aurell, J., & Gullett, B. K. (2013). Emission factors from aerial and ground measurements of field
 and laboratory forest burns in the southeastern U.S.: PM2.5, black and brown carbon, VOC,
 and PCDD/PCDF. Environmental Science and Technology, 47(15), 8443–8452.
 https://doi.org/10.1021/es402101k
- Barmet, P., Dommen, J., DeCarlo, P. F., Tritscher, T., Praplan, A. P., Platt, S. M., Prévôt, A. S. H.,
 Donahue, N. M., & Baltensperger, U. (2012). OH clock determination by proton transfer
 reaction mass spectrometry at an environmental chamber. *Atmospheric Measurement Techniques*, *5*(3), 647–656. https://doi.org/10.5194/amt-5-647-2012
- Bateman, A. P., Walser, M. L., Desyaterik, Y., Laskin, J., Laskin, A., & Nizkorodov, S. A. (2008). The
 effect of solvent on the analysis of secondary organic aerosol using electrospray ionization
 mass spectrometry. *Environmental Science and Technology*, 42(19), 7341–7346.
 https://doi.org/10.1021/es801226w
- Black, R. R., Aurell, J., Holder, A., George, I. J., Gullett, B. K., Hays, M. D., Geron, C. D., & Tabor,
 D. (2016). Characterization of gas and particle emissions from laboratory burns of peat.
 Atmospheric Environment, 132, 49–57. https://doi.org/10.1016/j.atmosenv.2016.02.024
- 924 Bluvshtein, N., Lin, P., Michel Flores, J., Segev, L., Mazar, Y., Tas, E., Snider, G., Weagle, C.,
 925 Brown, S. S., Laskin, A., & Rudich, Y. (2017). Broadband optical properties of biomass926 burning aerosol and identification of brown carbon chromophores. *Journal of Geophysical*927 *Research*, 122(10), 5441–5456. https://doi.org/10.1002/2016JD026230





- 928 Bond, T. C., & Bergstrom, R. W. (2006). Light absorption by carbonaceous particles: An 929 investigative review. In Aerosol Science and Technology (Vol. 40, Issue 1, pp. 27-67). 930 https://doi.org/10.1080/02786820500421521
- 931 Bond, T. C., Doherty, S. J., Fahey, D. W., Forster, P. M., Berntsen, T., DeAngelo, B. J., Flanner, M.
- 932 G., Ghan, S., Kärcher, B., Koch, D., Kinne, S., Kondo, Y., Quinn, P. K., Sarofim, M. C.,
- 933 Schultz, M. G., Schulz, M., Venkataraman, C., Zhang, H., Zhang, S., ... Zender, C. S. (2013).
- 934 Bounding the role of black carbon in the climate system: A scientific assessment. Journal of 935 Geophysical Research: Atmospheres, 118(11), 5380-5552. https://doi.org/10.1002/jgrd.50171
- 936 Bond, T., Venkataraman, C., & Masera, O. (2004). Global atmospheric impacts of residential fuels. 937 Energy for Sustainable Development, 8(3), 20–32. https://doi.org/10.1016/S0973-938 0826(08)60464-0
- 939 Bosch, C., Andersson, A., Kirillova, E. N., Budhavant, K., Tiwari, S., Praveen, P. S., Russell, L. M., 940 Beres, N. D., Ramanathan, V., & Gustafsson, Ö. (2014). Source-diagnostic dual-isotope
- 941 composition and optical properties of water-soluble organic carbon and elemental carbon in 942 the South Asian outflow intercepted over the Indian Ocean. Journal of Geophysical Research:
- 943 Atmospheres, 119(20), 11,743-11,759. https://doi.org/10.1002/2014JD022127
- 944 Brown, H., Liu, X., Feng, Y., Jiang, Y., Wu, M., Lu, Z., Wu, C., Murphy, S., & Pokhrel, R. (2018).
- 945 Radiative effect and climate impacts of brown carbon with the Community Atmosphere Model
- 946 (CAM5). Atmospheric Chemistry and Physics, 18(24), 17745–17768.
- 947 https://doi.org/10.5194/acp-18-17745-2018
- 948 Budisulistiorini, S. H., Riva, M., Williams, M., Chen, J., Itoh, M., Surratt, J. D., & Kuwata, M. (2017).
- 949 Light-Absorbing Brown Carbon Aerosol Constituents from Combustion of Indonesian Peat and
- 950 Biomass. Environmental Science and Technology, 51(8), 4415–4423.
- 951 https://doi.org/10.1021/acs.est.7b00397
- 952 Calderon-Arrieta, D., Morales, A. C., Hettiyadura, A. P. S., Estock, T. M., Li, C., Rudich, Y., & 953 Laskin, A. (2024). Enhanced Light Absorption and Elevated Viscosity of Atmospheric Brown
- 954 Carbon through Evaporation of Volatile Components. Environmental Science and Technology,
- 955 58(17), 7493-7504. https://doi.org/10.1021/acs.est.3c10184
- 956 Cao, T., Li, M., Zou, C., Fan, X., Song, J., Jia, W., Yu, C., Yu, Z., & Peng, P. (2021). Chemical 957 composition, optical properties, and oxidative potential of water- and methanol-soluble organic 958 compounds emitted from the combustion of biomass materials and coal. Atmospheric
- 959 Chemistry and Physics, 21(17), 13187-13205. https://doi.org/10.5194/acp-21-13187-2021
- 960 Chakrabarty, R. K., Gyawali, M., Yatavelli, R. L. N., Pandey, A., Watts, A. C., Knue, J., Chen, L. W. 961 A., Pattison, R. R., Tsibart, A., Samburova, V., & Moosmüller, H. (2016). Brown carbon
- 962 aerosols from burning of boreal peatlands: Microphysical properties, emission factors, and 963 implications for direct radiative forcing. Atmospheric Chemistry and Physics, 16(5), 3033-
- 3040. https://doi.org/10.5194/acp-16-3033-2016 964
- 965 Chakrabarty, R. K., Moosmüller, H., Chen, L. W. A., Lewis, K., Arnott, W. P., Mazzoleni, C., Dubey, 966 M. K., Wold, C. E., Hao, W. M., & Kreidenweis, S. M. (2010). Brown carbon in tar balls from 967 smoldering biomass combustion. Atmospheric Chemistry and Physics, 10(13), 6363–6370.
- 968 https://doi.org/10.5194/acp-10-6363-2010
- 969 Chakrabarty, R. K., Shetty, N. J., Thind, A. S., Beeler, P., Sumlin, B. J., Zhang, C., Liu, P., Idrobo, J.
- 970 C., Adachi, K., Wagner, N. L., Schwarz, J. P., Ahern, A., Sedlacek, A. J., Lambe, A., Daube,
- 971 C., Lyu, M., Liu, C., Herndon, S., Onasch, T. B., & Mishra, R. (2023). Shortwave absorption by





- 972 wildfire smoke dominated by dark brown carbon. *Nature Geoscience*, 16(8), 683–688.
- 973 https://doi.org/10.1038/s41561-023-01237-9
- 974 Chen, K., Raeofy, N., Lum, M., Mayorga, R., Woods, M., Bahreini, R., Zhang, H., & Lin, Y. H.
- 975 (2022). Solvent effects on chemical composition and optical properties of extracted secondary
- 976 brown carbon constituents. Aerosol Science and Technology, 56(10), 917–930.
- 977 https://doi.org/10.1080/02786826.2022.2100734
- 978 Chen, Y., & Bond, T. C. (2010). Light absorption by organic carbon from wood combustion.
- 979 Atmospheric Chemistry and Physics, 10(4), 1773–1787. https://doi.org/10.5194/acp-10-1773-980
 2010
- 981 Cheng, Y., He, K., Engling, G., Weber, R., Liu, J., Du, Z., & Dong, S. (2017). Brown and black
- carbon in Beijing aerosol: Implications for the effects of brown coating on light absorption by
- 983 black carbon. Science of The Total Environment, 599–600, 1047–1055.
- 984 https://doi.org/10.1016/j.scitotenv.2017.05.061
- China, S., Mazzoleni, C., Gorkowski, K., Aiken, A. C., & Dubey, M. K. (2013). Morphology and
- 986 mixing state of individual freshly emitted wildfire carbonaceous particles. Nature
- 987 Communications, 4. https://doi.org/10.1038/ncomms3122
- Chow, J. C., Watson, J. G., Chen, L.-W. A., Chang, M. C. O., Robinson, N. F., Trimble, D., & Kohl,
- 989 S. (2007). The IMPROVE A Temperature Protocol for Thermal/Optical Carbon Analysis:
- 990 Maintaining Consistency with a Long-Term Database. Journal of the Air & Waste Management
- 991 Association, 57(9), 1014–1023. https://doi.org/10.3155/1047-3289.57.9.1014
- 992 Christian, T. J., Kleiss, B., Yokelson, R. J., Holzinger, R., Crutzen, P. J., Hao, W. M., Saharjo, B. H.,
- 993 & Ward, D. E. (2003). Comprehensive laboratory measurements of biomass-burning
- 994 emissions: 1. Emissions from Indonesian, African, and other fuels. Journal of Geophysical
- 995 Research: Atmospheres, 108(D23), 4719. https://doi.org/10.1029/2003jd003704
- 996 Costa, H., De Rigo, D., Libertà, G., Houston Durrant, T., & San-Miguel-Ayanz, J. (2020). European
- 997 wildfire danger and vulnerability in a changing climate Towards integrating risk dimensions –
- 998 JRC PESETA IV project Task 9 forest fires. Publications Office of the European Union.
- 999 https://doi.org/10.2760/46951
- 1000 De Rigo, D., Libertà, G., Houston Durrant, T., Artés Vivancos, T., & San-Miguel-Ayanz, J. (2017).
- 1001 Forest fire danger extremes in Europe under climate change Variability and uncertainty.
- 1002 Publications Office of the European Union. https://doi.org/10.2760/13180
- 1003 Feyen, L., Ciscar, J., Gosling, S., Ibarreta, D., & Soria, A. (2020). Climate change impacts and
- 1004 adaptation in Europe JRC PESETA IV final report (D. Ibarreta & A. Soria, Eds.). Publications
- 1005 Office. https://doi.org/10.2760/171121
- 1006 Corbin, J. C., Modini, R. L., & Gysel-Beer, M. (2023). Mechanisms of soot-aggregate restructuring
- and compaction. Aerosol Science and Technology, 57(2), 89–111.
- 1008 https://doi.org/10.1080/02786826.2022.2137385
- 1009 De Groot, W. J., Flannigan, M. D., & Cantin, A. S. (2013). Climate change impacts on future boreal
- fire regimes. Forest Ecology and Management, 294, 35–44.
- 1011 https://doi.org/10.1016/j.foreco.2012.09.027
- 1012 Desgroux, P., Mercier, X., & Thomson, K. A. (2013). Study of the formation of soot and its
- precursors in flames using optical diagnostics. Proceedings of the Combustion Institute, 34(1),
- 1014 1713–1738. https://doi.org/10.1016/j.proci.2012.09.004





- 1015 Engling, G., Carrico, C. M., Kreidenweis, S. M., Collett Jr., J. L., Day, D. E., Malm, W. C., Lincoln,
- 1016 E., Min Hao, W., Iinuma, Y., & Herrmann, H. (2006). Determination of levoglucosan in biomass
- 1017 combustion aerosol by high-performance anion-exchange chromatography with pulsed
- amperometric detection. Atmospheric Environment, 40, 299–311.
- 1019 https://doi.org/10.1016/j.atmosenv.2005.12.069
- 1020 Faccinetto, A., Desgroux, P., Ziskind, M., Therssen, E., & Focsa, C. (2011). High-sensitivity
- detection of polycyclic aromatic hydrocarbons adsorbed onto soot particles using laser
- 1022 desorption/laser ionization/time-of-flight mass spectrometry: An approach to studying the soot
- inception process in low-pressure flames. Combustion and Flame, 158(2), 227–239.
- 1024 https://doi.org/10.1016/j.combustflame.2010.08.012
- 1025 Fan, X., Li, M., Cao, T., Cheng, C., Li, F., Xie, Y., Wei, S., Song, J., & Peng, P. (2018). Optical
- 1026 properties and oxidative potential of water- and alkaline-soluble brown carbon in smoke
- particles emitted from laboratory simulated biomass burning. Atmospheric Environment, 194,
- 1028 48–57. https://doi.org/10.1016/j.atmosenv.2018.09.025
- 1029 Fleming, L. T., Lin, P., Roberts, J. M., Selimovic, V., Yokelson, R., Laskin, J., Laskin, A., &
- 1030 Nizkorodov, S. A. (2020). Molecular composition and photochemical lifetimes of brown carbon
- 1031 chromophores in biomass burning organic aerosol. Atmospheric Chemistry and Physics,
- 1032 20(2), 1105–1129. https://doi.org/10.5194/acp-20-1105-2020
- 1033 Hallar, A. G., Lowenthal, D. H., Clegg, S. L., Samburova, V., Taylor, N., Mazzoleni, L. R., Zielinska,
- 1034 B. K., Kristensen, T. B., Chirokova, G., McCubbin, I. B., Dodson, C., & Collins, D. (2013).
- 1035 Chemical and hygroscopic properties of aerosol organics at Storm Peak Laboratory. *Journal*
- of Geophysical Research: Atmospheres, 118(10), 4767–4779.
- 1037 https://doi.org/10.1002/jgrd.50373
- Hartikainen, A., Tiitta, P., Ihalainen, M., Yli-Pirilä, P., Orasche, J., Czech, H., Kortelainen, M.,
- 1039 Lamberg, H., Suhonen, H., Koponen, H., Hao, L., Zimmermann, R., Jokiniemi, J., Tissari, J., &
- 1040 Sippula, O. (2020). Photochemical transformation of residential wood combustion emissions:
- 1041 Dependence of organic aerosol composition on OH exposure. Atmospheric Chemistry and
- 1042 Physics, 20(11), 6357–6378. https://doi.org/10.5194/acp-20-6357-2020
- 1043 Hecobian, A., Zhang, X., Zheng, M., Frank, N., Edgerton, E. S., & Weber, R. J. (2010). Water-
- 1044 Soluble Organic Aerosol material and the light-absorption characteristics of aqueous extracts
- measured over the Southeastern United States. Atmospheric Chemistry and Physics, 10(13),
- 1046 5965–5977. https://doi.org/10.5194/acp-10-5965-2010
- 1047 Hems, R. F., Schnitzler, E. G., Bastawrous, M., Soong, R., Simpson, A. J., & Abbatt, J. P. D.
- 1048 (2020). Aqueous Photoreactions of Wood Smoke Brown Carbon. ACS Earth and Space
- 1049 *Chemistry*, 4(7), 1149–1160. https://doi.org/10.1021/acsearthspacechem.0c00117
- Hems, R. F., Schnitzler, E. G., Liu-Kang, C., Cappa, C. D., & Abbatt, J. P. D. (2021). Aging of
- 1051 Atmospheric Brown Carbon Aerosol. ACS Earth and Space Chemistry, 5(4), 722–748.
- https://doi.org/10.1021/acsearthspacechem.0c00346
- Hennigan, C. J., Miracolo, M. A., Engelhart, G. J., May, A. A., Presto, A. A., Lee, T., Sullivan, A. P.,
- 1054 McMeeking, G. R., Coe, H., Wold, C. E., Hao, W. M., Gilman, J. B., Kuster, W. C., De Gouw,
- 1055 J., Schichtel, B. A., Collett, J. L., Kreidenweis, S. M., & Robinson, A. L. (2011). Chemical and
- 1056 physical transformations of organic aerosol from the photo-oxidation of open biomass burning
- 1057 emissions in an environmental chamber. Atmospheric Chemistry and Physics, 11(15), 7669–
- 1058 7686. https://doi.org/10.5194/acp-11-7669-2011



1099

1100



1059 Hoffer, A., Tóth, A., NyirÅ'-Kósa, I., Pósfai, M., & Gelencsér, A. (2016). Light absorption properties 1060 of laboratory-generated tar ball particles, Atmospheric Chemistry and Physics, 16(1), 239-1061 246. https://doi.org/10.5194/acp-16-239-2016 1062 Hoffer, A., Tóth, Á., Pósfai, M., Chung, C. E., & Gelencsér, A. (2017), Brown carbon absorption in 1063 the red and near-infrared spectral region. Atmospheric Measurement Techniques, 10(6), 2353-2359. https://doi.org/10.5194/amt-10-2353-2017 1064 1065 Huang, R. J., Yang, L., Cao, J., Chen, Y., Chen, Q., Li, Y., Duan, J., Zhu, C., Dai, W., Wang, K., Lin, 1066 C., Ni, H., Corbin, J. C., Wu, Y., Zhang, R., Tie, X., Hoffmann, T., O'Dowd, C., & Dusek, U. 1067 (2018). Brown Carbon Aerosol in Urban Xi'an, Northwest China: The Composition and Light 1068 Absorption Properties. Environmental Science and Technology, 52(12), 6825-6833. 1069 https://doi.org/10.1021/acs.est.8b02386 1070 Huo, Y., Li, M., Jiang, M., & Qi, W. (2018). Light absorption properties of HULIS in primary 1071 particulate matter produced by crop straw combustion under different moisture contents and 1072 stacking modes. Atmospheric Environment, 191, 490-499. 1073 https://doi.org/10.1016/j.atmosenv.2018.08.038 1074 Ihalainen, M., Jalava, P., Ihantola, T., Kasurinen, S., Uski, O., Sippula, O., Hartikainen, A., Tissari, J., Kuuspalo, K., Lähde, A., Hirvonen, M.-R., & Jokiniemi, J. (2019a). Design and validation of 1075 1076 an air-liquid interface (ALI) exposure device based on thermophoresis. Aerosol Science and Technology, 53(2), 133-145. https://doi.org/10.1080/02786826.2018.1556775 1077 1078 Ihalainen, M., Tiitta, P., Czech, H., Yli-Pirilä, P., Hartikainen, A., Kortelainen, M., Tissari, J., Stengel, 1079 B., Sklorz, M., Suhonen, H., Lamberg, H., Leskinen, A., Kiendler-Scharr, A., Harndorf, H., 1080 Zimmermann, R., Jokiniemi, J., & Sippula, O. (2019b). A novel high-volume Photochemical 1081 Emission Aging flow tube Reactor (PEAR). Aerosol Science and Technology, 53(3), 276–294. 1082 https://doi.org/10.1080/02786826.2018.1559918 1083 linuma, Y., Brüggemann, E., Gnauk, T., Müller, K., Andreae, M. O., Helas, G., Parmar, R., & 1084 Herrmann, H. (2007a), Source characterization of biomass burning particles: The combustion 1085 of selected European conifers, African hardwood, savanna grass, and German and 1086 Indonesian peat. Journal of Geophysical Research: Atmospheres, 112(D8), D08209. https://doi.org/10.1029/2006JD007120 1087 1088 Jacobson, M. Z. (2000). A physically-based treatment of elemental carbon optics: Implications for global direct forcing of aerosols. Geophysical Research Letters, 27(2), 217-220. 1089 1090 https://doi.org/10.1029/1999GL010968 1091 Jacobson, M. Z. (2001). Strong radiative heating due to the mixing state of black carbon in 1092 atmospheric aerosols. Nature, 409(6821), 695-697. https://doi.org/10.1038/35055518 1093 Jayarathne, T., Stockwell, C. E., Gilbert, A. A., Daugherty, K., Cochrane, M. A., Ryan, K. C., Putra, E. I., Saharjo, B. H., Nurhayati, A. D., Albar, I., Yokelson, R. J., & Stone, E. A. (2018). 1094 1095 Chemical characterization of fine particulate matter emitted by peat fires in Central Kalimantan, Indonesia, during the 2015 El Niño. Atmospheric Chemistry and Physics, 18(4), 1096 1097 2585-2600. https://doi.org/10.5194/acp-18-2585-2018

Jennings, S. G., Pinnick, R. G., & Gillespie, J. B. (1979). Relation between absorption coefficient

and imaginary index of atmospheric aerosol constituents. Applied Optics, 18(9), 1368.

https://doi.org/10.1364/AO.18.001368





- Kirchstetter, T. W., Corrigan, C. E., & Novakov, T. (2001). Laboratory and field investigation of the adsorption of gaseous organic compounds onto guartz filters. *Atmospheric Environment*.
- 1103 35(9), 1663–1671. https://doi.org/10.1016/S1352-2310(00)00448-9
- 1104 Kirchstetter, T. W., Novakov, T., & Hobbs, P. V. (2004). Evidence that the spectral dependence of light absorption by aerosols is affected by organic carbon. *Journal of Geophysical Research:*
- 1106 Atmospheres, 109(D21), D21208. https://doi.org/10.1029/2004JD004999
- 1107 Kirillova, E. N., Andersson, A., Han, J., Lee, M., & Gustafsson, Ö. (2014). Sources and light
- absorption of water-soluble organic carbon aerosols in the outflow from northern China.
- 1109 Atmospheric Chemistry and Physics, 14(3), 1413–1422. https://doi.org/10.5194/acp-14-1413-
- 1110 <u>2014</u>
- 1111 Koch, B. P., & Dittmar, T. (2006). From mass to structure: an aromaticity index for high-resolution
- mass data of natural organic matter. Rapid Communications in Mass Spectrometry, 20(5),
- 1113 926–932. https://doi.org/10.1002/rcm.2386
- 1114 Kourtchev, I., Hellebust, S., Bell, J. M., O'Connor, I. P., Healy, R. M., Allanic, A., Healy, D., Wenger,
- 1115 J. C., & Sodeau, J. R. (2011). The use of polar organic compounds to estimate the
- 1116 contribution of domestic solid fuel combustion and biogenic sources to ambient levels of
- organic carbon and PM2.5 in Cork Harbour, Ireland. Science of The Total Environment,
- 1118 409(11), 2143–2155. https://doi.org/10.1016/j.scitotenv.2011.02.027
- Krawchuk, M. A., Cumming, S. G., & Flannigan, M. D. (2009). Predicted changes in fire weather
- suggest increases in lightning fire initiation and future area burned in the mixedwood boreal forest. *Climatic Change*, 92(1–2), 83–97. https://doi.org/10.1007/s10584-008-9460-7
- 1122 Kroll, J. H., Donahue, N. M., Jimenez, J. L., Kessler, S. H., Canagaratna, M. R., Wilson, K. R.,
- 1123 Altieri, K. E., Mazzoleni, L. R., Wozniak, A. S., Bluhm, H., Mysak, E. R., Smith, J. D., Kolb, C.
- 1124 E., & Worsnop, D. R. (2011). Carbon oxidation state as a metric for describing the chemistry
- of atmospheric organic aerosol. *Nature Chemistry*, 3(2), 133–139.
- 1126 https://doi.org/10.1038/nchem.948
- 1127 Kroll, J. H., Lim, C. Y., Kessler, S. H., & Wilson, K. R. (2015). Heterogeneous Oxidation of
- 1128 Atmospheric Organic Aerosol: Kinetics of Changes to the Amount and Oxidation State of
- 1129 Particle-Phase Organic Carbon. *The Journal of Physical Chemistry A*, 119(44), 10767–10783.
- 1130 https://doi.org/10.1021/acs.jpca.5b06946
- 1131 Kumar, N. K., Corbin, J. C., Bruns, E. A., Massabó, D., Slowik, J. G., Drinovec, L., Močnik, G.,
- 1132 Prati, P., Vlachou, A., Baltensperger, U., Gysel, M., El-Haddad, I., & Prévôt, A. S. H. (2018).
- 1133 Production of particulate brown carbon during atmospheric aging of residential wood-burning
- emissions. Atmospheric Chemistry and Physics, 18(24), 17843–17861.
- 1135 https://doi.org/10.5194/acp-18-17843-2018
- Lambe, A. T., Ahern, A. T., Williams, L. R., Slowik, J. G., Wong, J. P. S., Abbatt, J. P. D., Brune, W.
- 1137 H., Ng, N. L., Wright, J. P., Croasdale, D. R., Worsnop, D. R., Davidovits, P., & Onasch, T. B.
- 1138 (2011). Characterization of aerosol photooxidation flow reactors: heterogeneous oxidation,
- 1139 secondary organic aerosol formation and cloud condensation nuclei activity measurements.
- 1140 Atmospheric Measurement Techniques, 4(3), 445–461. https://doi.org/10.5194/amt-4-445-
- 1141 2011
- 1142 Lambe, A. T., Cappa, C. D., Massoli, P., Onasch, T. B., Forestieri, S. D., Martin, A. T., Cummings,
- 1143 M. J., Croasdale, D. R., Brune, W. H., Worsnop, D. R., & Davidovits, P. (2013). Relationship
- 1144 between oxidation level and optical properties of secondary organic aerosol. Environmental
- 1145 Science and Technology, 47(12), 6349–6357. https://doi.org/10.1021/es401043j





- 1146 Laskin, A., Laskin, J., & Nizkorodov, S. A. (2015). Chemistry of Atmospheric Brown Carbon.
- 1147 Chemical Reviews, 115(10), 4335–4382. https://doi.org/10.1021/cr5006167
- 1148 Leskinen, A., Yli-Pirilä, P., Kuuspalo, K., Sippula, O., Jalava, P., Hirvonen, M.-R., Jokiniemi, J.,
- 1149 Virtanen, A., Komppula, M., & Lehtinen, K. E. J. (2015). Characterization and testing of a new
- 1150 environmental chamber. Atmospheric Measurement Techniques, 8(6), 2267–2278.
- 1151 https://doi.org/10.5194/amt-8-2267-2015
- 1152 Leskinen, J., Hartikainen, A., Väätäinen, S., Ihalainen, M., Virkkula, A., Mesceriakovas, A., Tiitta, P.,
- 1153 Miettinen, M., Lamberg, H., Czech, H., Yli-Pirilä, P., Tissari, J., Jakobi, G., Zimmermann, R., &
- 1154 Sippula, O. (2023). Photochemical Aging Induces Changes in the Effective Densities,
- 1155 Morphologies, and Optical Properties of Combustion Aerosol Particles. *Environmental*
- 1156 Science and Technology, 57(13), 5137–5148. https://doi.org/10.1021/acs.est.2c04151
- 1157 Leskinen, J., Ihalainen, M., Torvela, T., Kortelainen, M., Lamberg, H., Tiitta, P., Jakobi, G.,
- 1158 Grigonyte, J., Joutsensaari, J., Sippula, O., Tissari, J., Virtanen, A., Zimmermann, R., &
- 1159 Jokiniemi, J. (2014). Effective density and morphology of particles emitted from small-scale
- 1160 combustion of various wood fuels. Environmental Science and Technology, 48(22), 13298–
- 1161 13306. https://doi.org/10.1021/es502214a
- 1162 Li, C., Chen, P., Kang, S., Yan, F., Hu, Z., Qu, B., & Sillanpää, M. (2016). Concentrations and light
- absorption characteristics of carbonaceous aerosol in PM 2.5 and PM 10 of Lhasa city, the
- 1164 Tibetan Plateau. *Atmospheric Environment*, 127, 340–346.
- 1165 https://doi.org/10.1016/j.atmosenv.2015.12.059
- 1166 Li, C., He, Q., Hettiyadura, A. P. S., Käfer, U., Shmul, G., Meidan, D., Zimmermann, R., Brown, S.
- 1167 S., George, C., Laskin, A., & Rudich, Y. (2019). Formation of secondary brown carbon in
- 1168 biomass burning aerosol proxies through no3 radical reactions. *Environmental Science and*
- 1169 Technology, 54(3), 1395–1405. https://doi.org/10.1021/acs.est.9b05641
- 1170 Li, X., Xiao, M., Xu, X., Zhou, J., Yang, K., Wang, Z., Zhang, W., Hopke, P. K., Hopke, P. K., Zhao,
- 1171 W., & Li, X. (2020). Light Absorption Properties of Organic Aerosol from Wood Pyrolysis:
- 1172 Measurement Method Comparison and Radiative Implications. Environmental Science and
- 1173 *Technology*, 54(12), 7156–7164. https://doi.org/10.1021/acs.est.0c01475
- 1174 Li, Y., Pöschl, U., & Shiraiwa, M. (2016). Molecular corridors and parameterizations of volatility in
- the chemical evolution of organic aerosols. Atmospheric Chemistry and Physics, 16(5), 3327–
- 1176 3344. https://doi.org/10.5194/acp-16-3327-2016
- 1177 Lin, P., Bluvshtein, N., Rudich, Y., Nizkorodov, S. A., Laskin, J., & Laskin, A. (2017). Molecular
- 1178 Chemistry of Atmospheric Brown Carbon Inferred from a Nationwide Biomass Burning Event.
- 1179 Environmental Science and Technology, 51(20), 11561–11570.
- 1180 https://doi.org/10.1021/acs.est.7b02276
- 1181 Lin, P., Rincon, A. G., Kalberer, M., & Yu, J. Z. (2012). Elemental Composition of HULIS in the
- 1182 Pearl River Delta Region, China: Results Inferred from Positive and Negative Electrospray
- 1183 High Resolution Mass Spectrometric Data. Environmental Science & Technology, 46(14),
- 1184 7454–7462. https://doi.org/10.1021/es300285d
- 1185 Liu, D., Whitehead, J., Alfarra, M. R., Reyes-Villegas, E., Spracklen, D. V., Reddington, C. L.,
- 1186 Kong, S., Williams, P. I., Ting, Y.-C., Haslett, S., Taylor, J. W., Flynn, M. J., Morgan, W. T.,
- 1187 McFiggans, G., Coe, H., & Allan, J. D. (2017). Black-carbon absorption enhancement in the
- atmosphere determined by particle mixing state. *Nature Geoscience*, 10(3), 184–188.
- 1189 https://doi.org/10.1038/ngeo2901





- 1190 Liu, J., Bergin, M., Guo, H., King, L., Kotra, N., Edgerton, E., & Weber, R. J. (2013). Size-resolved
- 1191 measurements of brown carbon in water and methanol extracts and estimates of their
- 1192 contribution to ambient fine-particle light absorption. Atmospheric Chemistry and Physics,
- 1193 13(24), 12389–12404. https://doi.org/10.5194/acp-13-12389-2013
- 1194 Liu, S., Aiken, A. C., Gorkowski, K., Dubey, M. K., Cappa, C. D., Williams, L. R., Herndon, S. C.,
- 1195 Massoli, P., Fortner, E. C., Chhabra, P. S., Brooks, W. A., Onasch, T. B., Jayne, J. T.,
- 1196 Worsnop, D. R., China, S., Sharma, N., Mazzoleni, C., Xu, L., Ng, N. L., ... Prévôt, A. S. H.
- 1197 (2015). Enhanced light absorption by mixed source black and brown carbon particles in UK
- 1198 winter. *Nature Communications*, 6. https://doi.org/10.1038/ncomms9435
- Lu, Z., Streets, D. G., Winijkul, E., Yan, F., Chen, Y., Bond, T. C., Feng, Y., Dubey, M. K., Liu, S.,
- 1200 Pinto, J. P., & Carmichael, G. R. (2015). Light absorption properties and radiative effects of
- 1201 primary organic aerosol emissions. Environmental Science and Technology, 49(8), 4868–
- 1202 4877. https://doi.org/10.1021/acs.est.5b00211
- Ma, J., Li, X., Gu, P., Dallmann, T. R., Presto, A. A., & Donahue, N. M. (2016). Estimating ambient
- 1204 particulate organic carbon concentrations and partitioning using thermal optical
- 1205 measurements and the volatility basis set. Aerosol Science and Technology, 50(6), 638–651.
- 1206 https://doi.org/10.1080/02786826.2016.1158778
- 1207 Martinsson, J., Eriksson, A. C., Nielsen, I. E., Malmborg, V. B., Ahlberg, E., Andersen, C., Lindgren,
- 1208 R., Nyström, R., Nordin, E. Z., Brune, W. H., Svenningsson, B., Swietlicki, E., Boman, C., &
- 1209 Pagels, J. H. (2015). Impacts of Combustion Conditions and Photochemical Processing on
- 1210 the Light Absorption of Biomass Combustion Aerosol. Environmental Science and
- 1211 Technology, 49(24), 14663–14671. https://doi.org/10.1021/acs.est.5b03205
- 1212 McCarty, J. L., Aalto, J., Paunu, V.-V., Arnold, S. R., Eckhardt, S., Klimont, Z., Fain, J. J.,
- 1213 Evangeliou, N., Venäläinen, A., Tchebakova, N. M., Parfenova, E. I., Kupiainen, K., Soja, A. J.,
- 1214 Huang, L., & Wilson, S. (2021). Reviews and syntheses: Arctic fire regimes and emissions in
- 1215 the 21st century. *Biogeosciences*, 18(18), 5053–5083. https://doi.org/10.5194/bg-18-5053-
- 1216 2021
- 1217 McClure, C. D., Lim, C. Y., Hagan, D. H., Kroll, J. H., & Cappa, C. D. (2020). Biomass-burning-
- derived particles from a wide variety of fuels Part 1: Properties of primary particles.
- 1219 Atmospheric Chemistry and Physics, 20(3), 1531–1547. https://doi.org/10.5194/acp-20-1531-
- 1220 2020
- 1221 McIntyre, C., & McRae, C. (2005). Proposed guidelines for sample preparation and ESI-MS
- analysis of humic substances to avoid self-esterification. *Organic Geochemistry*, 36(4), 543–
- 1223 553. https://doi.org/10.1016/j.orggeochem.2004.11.002
- 1224 McMeeking, G. R., Fortner, E., Onasch, T. B., Taylor, J. W., Flynn, M., Coe, H., & Kreidenweis, S.
- 1225 M. (2014). Impacts of nonrefractory material on light absorption by aerosols emitted from
- biomass burning. *Journal of Geophysical Research: Atmospheres*, 119(21), 12,272-12,286.
- 1227 https://doi.org/10.1002/2014JD021750
- 1228 Mo, Y., Li, J., Liu, J., Zhong, G., Cheng, Z., Tian, C., Chen, Y., & Zhang, G. (2017). The influence of
- 1229 solvent and pH on determination of the light absorption properties of water-soluble brown
- 1230 carbon. Atmospheric Environment, 161, 90–98.
- 1231 https://doi.org/10.1016/j.atmosenv.2017.04.037
- 1232 Moosmüller, H., Chakrabarty, R. K., & Arnott, W. P. (2009). Aerosol light absorption and its
- 1233 measurement: A review. Journal of Quantitative Spectroscopy and Radiative Transfer,
- 1234 110(11), 844–878. https://doi.org/10.1016/j.jqsrt.2009.02.035





- 1235 Moosmüller, H., Chakrabarty, R. K., Ehlers, K. M., & Arnott, W. P. (2011). Absorption Ångström
- 1236 coefficient, brown carbon, and aerosols: Basic concepts, bulk matter, and spherical particles.
- 1237 Atmospheric Chemistry and Physics, 11(3), 1217–1225. https://doi.org/10.5194/acp-11-1217-
- 1238 2011
- 1239 Moschos, V., Christensen, C., Mouton, M., Fiddler, M. N., Isolabella, T., Mazzei, F., Massabò, D.,
- 1240 Turpin, B. J., Bililign, S., & Surratt, J. D. (2024). Quantifying the Light-Absorption Properties
- 1241 and Molecular Composition of Brown Carbon Aerosol from Sub-Saharan African Biomass
- 1242 Combustion. Environmental Science and Technology, 58(9), 4268–4280.
- 1243 https://doi.org/10.1021/acs.est.3c09378
- 1244 Moschos, V., Kumar, N. K., Daellenbach, K. R., Baltensperger, U., Prévôt, A. S. H., & El Haddad, I.
- 1245 (2018). Source Apportionment of Brown Carbon Absorption by Coupling Ultraviolet–Visible
- 1246 Spectroscopy with Aerosol Mass Spectrometry. *Environmental Science & Technology Letters*,
- 1247 5(6), 302–308. https://doi.org/10.1021/acs.estlett.8b00118
- 1248 Mukherjee, A., Dey, S., Rana, A., Jia, S., Banerjee, S., & Sarkar, S. (2020). Sources and
- atmospheric processing of brown carbon and HULIS in the Indo-Gangetic Plain: Insights from
- 1250 compositional analysis. *Environmental Pollution*, 267.
- 1251 https://doi.org/10.1016/j.envpol.2020.115440
- 1252 Mukherjee, A., Hartikainen, A., Joutsensaari, J., Basnet, S., Mesceriakovas, A., Ihalainen, M., Yli-
- 1253 Pirilä, P., Leskinen, J., Somero, M., Louhisalmi, J., Fang, Z., Kalberer, M., Rudich, Y., Tissari,
- 1254 J., Czech, H., Zimmermann, R., & Sippula, O. (2024). Black carbon and particle lung-
- 1255 deposited surface area in residential wood combustion emissions: Effects of an electrostatic
- 1256 precipitator and photochemical aging. Science of The Total Environment, 952, 175840.
- 1257 https://doi.org/10.1016/j.scitotenv.2024.175840
- 1258 Navinya, C., Kapoor, T. S., Anurag, G., Venkataraman, C., Phuleria, H. C., & Chakrabarty, R. K.
- 1259 (2024). Brownness of Organics in Anthropogenic Biomass Burning Aerosols over South Asia.
- 1260 https://doi.org/10.5194/egusphere-2024-1313
- 1261 Park, S. S., & Yu, J. (2016). Chemical and light absorption properties of humic-like substances
- 1262 from biomass burning emissions under controlled combustion experiments. *Atmospheric*
- 1263 Environment, 136, 114–122. https://doi.org/10.1016/j.atmosenv.2016.04.022
- 1264 Phillips, C. A., Rogers, B. M., Elder, M., Cooperdock, S., Moubarak, M., Randerson, J. T., &
- 1265 Frumhoff, P. C. (2022). Escalating carbon emissions from North American boreal forest
- 1266 wildfires and the climate mitigation potential of fire management. Science Advances, 8(17).
- 1267 https://doi.org/10.1126/sciadv.abl7161
- Phillips, S. M., & Smith, G. D. (2017). Spectroscopic comparison of water- and methanol-soluble
- 1269 brown carbon particulate matter. Aerosol Science and Technology, 51(9), 1113–1121.
- 1270 https://doi.org/10.1080/02786826.2017.1334109
- 1271 Pokhrel, R. P., Wagner, N. L., Langridge, J. M., Lack, D. A., Jayarathne, T., Stone, E. A., Stockwell,
- 1272 C. E., Yokelson, R. J., & Murphy, S. M. (2016). Parameterization of single-scattering albedo
- 1273 (SSA) and absorption Ångström exponent (AAE) with EC / OC for aerosol emissions from
- biomass burning. *Atmospheric Chemistry and Physics*, *16*(15), 9549–9561.
- 1275 https://doi.org/10.5194/acp-16-9549-2016
- 1276 Popovicheva, O. B., Engling, G., Ku, I.-T., Timofeev, M. A., & Shonija, N. K. (2019). Aerosol
- 1277 Emissions from Long-lasting Smoldering of Boreal Peatlands: Chemical Composition,
- Markers, and Microstructure. *Aerosol and Air Quality Research*, 19(3), 484–503.
- 1279 https://doi.org/10.4209/aaqr.2018.08.0302





- Rogers, B. M., Soja, A. J., Goulden, M. L., & Randerson, J. T. (2015). Influence of tree species on continental differences in boreal fires and climate feedbacks. *Nature Geoscience*, 8(3), 228–
- 1282 234. https://doi.org/10.1038/ngeo2352
- Rüger, C. P., Le Maître, J., Riches, E., Palmer, M., Orasche, J., Sippula, O., Jokiniemi, J., Afonso,
- 1284 C., Giusti, P., & Zimmermann, R. (2021). Cyclic Ion Mobility Spectrometry Coupled to High-
- 1285 Resolution Time-of-Flight Mass Spectrometry Equipped with Atmospheric Solid Analysis
 1286 Probe for the Molecular Characterization of Combustion Particulate Matter. *Journal of the*
- 1286 Prope for the Molecular Characterization of Compustion Particulate Matter. *Journal of the*
- 1287 American Society for Mass Spectrometry, 32(1), 206–217.
- 1288 https://doi.org/10.1021/jasms.0c00274
- Saleh, R. (2020). From Measurements to Models: Toward Accurate Representation of Brown
 Carbon in Climate Calculations. In *Current Pollution Reports* (Vol. 6, Issue 2, pp. 90–104).
 Springer. https://doi.org/10.1007/s40726-020-00139-3
- Saleh, R., Cheng, Z., & Atwi, K. (2018). The Brown-Black Continuum of Light-Absorbing
 Combustion Aerosols. *Environmental Science and Technology Letters*, *5*(8), 508–513.
 https://doi.org/10.1021/acs.estlett.8b00305
- Saleh, R., Robinson, E. S., Tkacik, D. S., Ahern, A. T., Liu, S., Aiken, A. C., Sullivan, R. C., Presto,
 A. A., Dubey, M. K., Yokelson, R. J., Donahue, N. M., & Robinson, A. L. (2014). Brownness of
 organics in aerosols from biomass burning linked to their black carbon content. *Nature Geoscience*, 7(9), 647–650. https://doi.org/10.1038/ngeo2220
- Schneider, E., Rüger, C. P., Chacón-Patiño, M. L., Somero, M., Ruppel, M. M., Ihalainen, M., Köster, K., Sippula, O., Czech, H., & Zimmermann, R. (2024a). The complex composition of organic aerosols emitted during burning varies between Arctic and boreal peat.

 Communications Earth and Environment, 5(1). https://doi.org/10.1038/s43247-024-01304-y
- Schneider, E., Czech, H., Hartikainen, A., Hansen, H. J., Gawlitta, N., Ihalainen, M., Yli-Pirilä, P., Somero, M., Kortelainen, M., Louhisalmi, J., Orasche, J., Fang, Z., Rudich, Y., Sippula, O., Rüger, C. P., & Zimmermann, R. (2024b). Molecular composition of fresh and aged aerosols
- from residential wood combustion and gasoline car with modern emission mitigation
- 1307 technology. *Environmental Science: Processes & Impacts*, 26(8), 1295–1309.
- 1307 technology. Environmental Science. Processes & Impacis, 20(6), 1293–1308
- 1308 https://doi.org/10.1039/D4EM00106K
- Sedlacek, A. J., Buseck, P. R., Adachi, K., Onasch, T. B., Springston, S. R., & Kleinman, L. (2018).
 Formation and evolution of tar balls from northwestern US wildfires. *Atmospheric Chemistry* and Physics, 18(15), 11289–11301. https://doi.org/10.5194/acp-18-11289-2018
- Seinfeld, J.H. and Pandis, S.N. (2006) Atmospheric Chemistry and Physics: From Air Pollution to Climate Change. 2nd Edition, John Wiley & Sons, New York.
- Sengupta, D., Samburova, V., Bhattarai, C., Kirillova, E., Mazzoleni, L., Iaukea-Lum, M., Watts, A., Moosmüller, H., & Khlystov, A. (2018). Light absorption by polar and non-polar aerosol
- 1316 compounds from laboratory biomass combustion. *Atmospheric Chemistry and Physics*,
- 1317 *18*(15), 10849–10867. https://doi.org/10.5194/acp-18-10849-2018
- 1318 Shetty, N. J., Pandey, A., Baker, S., Hao, W. M., & Chakrabarty, R. K. (2019). Measuring light absorption by freshly emitted organic aerosols: Optical artifacts in traditional solvent-
- 1320 extraction-based methods. Atmospheric Chemistry and Physics, 19(13), 8817–8830.
- 1321 https://doi.org/10.5194/acp-19-8817-2019
- Smith, D. M., Fiddler, M. N., Pokhrel, R. P., & Bililign, S. (2020). Laboratory studies of fresh and aged biomass burning aerosol emitted from east African biomass fuels Part 1: Optical





1324 properties. Atmospheric Chemistry and Physics, 20(17), 10149–10168. 1325 https://doi.org/10.5194/acp-20-10149-2020 1326 Solum, M. S., Sarofim, A. F., Pugmire, R. J., Fletcher, T. H., & Zhang, H. (2001). 13 C NMR 1327 Analysis of Soot Produced from Model Compounds and a Coal. Energy & Fuels, 15(4), 961-1328 971. https://doi.org/10.1021/ef0100294 1329 Stockwell, C. E., Jayarathne, T., Cochrane, M. A., Ryan, K. C., Putra, E. I., Saharjo, B. H., 1330 Nurhayati, A. D., Albar, I., Blake, D. R., Simpson, I. J., Stone, E. A., & Yokelson, R. J. (2016). 1331 Field measurements of trace gases and aerosols emitted by peat fires in Central Kalimantan, 1332 Indonesia, during the 2015 El Niño. Atmospheric Chemistry and Physics, 16(18), 11711-1333 11732. https://doi.org/10.5194/acp-16-11711-2016 1334 Stockwell, C. E., Veres, P. R., Williams, J., & Yokelson, R. J. (2015). Characterization of biomass 1335 burning emissions from cooking fires, peat, crop residue, and other fuels with high-resolution 1336 proton-transfer-reaction time-of-flight mass spectrometry. Atmospheric Chemistry and 1337 Physics, 15(2), 845-865. https://doi.org/10.5194/acp-15-845-2015 1338 Stockwell, C. E., Yokelson, R. J., Kreidenweis, S. M., Robinson, A. L., DeMott, P. J., Sullivan, R. C., 1339 Reardon, J., Ryan, K. C., Griffith, D. W. T., & Stevens, L. (2014). Trace gas emissions from 1340 combustion of peat, crop residue, domestic biofuels, grasses, and other fuels: configuration 1341 and Fourier transform infrared (FTIR) component of the fourth Fire Lab at Missoula 1342 Experiment (FLAME-4). Atmospheric Chemistry and Physics, 14(18), 9727–9754. 1343 https://doi.org/10.5194/acp-14-9727-2014 1344 Sumlin, B. J., Heinson, Y. W., Shetty, N., Pandey, A., Pattison, R. S., Baker, S., Hao, W. M., & 1345 Chakrabarty, R. K. (2018). UV-Vis-IR spectral complex refractive indices and optical 1346 properties of brown carbon aerosol from biomass burning. Journal of Quantitative 1347 Spectroscopy and Radiative Transfer, 206, 392–398. 1348 https://doi.org/10.1016/j.jqsrt.2017.12.009 Sumlin, B. J., Pandey, A., Walker, M. J., Pattison, R. S., Williams, B. J., & Chakrabarty, R. K. 1349 1350 (2017). Atmospheric Photooxidation Diminishes Light Absorption by Primary Brown Carbon 1351 Aerosol from Biomass Burning. Environmental Science & Technology Letters, 4(12), 540-545. 1352 https://doi.org/10.1021/acs.estlett.7b00393 1353 Taylor, N. F., Collins, D. R., Lowenthal, D. H., McCubbin, I. B., Hallar, A. G., Samburova, V., 1354 Zielinska, B., Kumar, N., & Mazzoleni, L. R. (2017). Hygroscopic growth of water soluble 1355 organic carbon isolated from atmospheric aerosol collected at US national parks and Storm 1356 Peak Laboratory. Atmospheric Chemistry and Physics, 17(4), 2555–2571. 1357 https://doi.org/10.5194/acp-17-2555-2017 1358 Urbanski, S. P. (2013). Combustion efficiency and emission factors for wildfire-season fires in 1359 mixed conifer forests of the northern Rocky Mountains, US. Atmospheric Chemistry and Physics, 13(14), 7241-7262. https://doi.org/10.5194/acp-13-7241-2013 1360 1361 Vakkari, V., Beukes, J. P., Dal Maso, M., Aurela, M., Josipovic, M., & van Zyl, P. G. (2018). Major 1362 secondary aerosol formation in southern African open biomass burning plumes. Nature 1363 Geoscience, 11(8), 580-583. https://doi.org/10.1038/s41561-018-0170-0 1364 Vakkari, V., Vettikkat, L., Kommula, S., Mukherjee, A., Hao, L., Backman, J., Buchholz, A., Gawlitta, 1365 N., Ihalainen, M., Jaars, K., Köster, K., Le, V., Miettinen, P., Nissinen, A., Czech, H., Alton, M., Passig, J., Peltokorpi, S., Piedehierro, A. A., Pullinen, I., Rosewig, E. I., Schobesberger, S., 1366 1367 Shukla, D., Siebert, S. J., Somero, M., Virkkula, A., Welti, A., Yli-Pirilä, P., Ylisirniö, A., 1368 Zimmermann, R., van Zyl, P. G., Virtanen, A., & Sippula, O. (2025). Laboratory experiments





- 1369 on savannah and European boreal forest fire emissions. Journal of Geophysical Research:
- 1370 Atmospheres, under revision
- 1371 Walker, X. J., Rogers, B. M., Veraverbeke, S., Johnstone, J. F., Baltzer, J. L., Barrett, K.,
- 1372 Bourgeau-Chavez, L., Day, N. J., de Groot, W. J., Dieleman, C. M., Goetz, S., Hoy, E.,
- 1373 Jenkins, L. K., Kane, E. S., Parisien, M.-A., Potter, S., Schuur, E. A. G., Turetsky, M.,
- 1374 Whitman, E., & Mack, M. C. (2020). Fuel availability not fire weather controls boreal wildfire
- severity and carbon emissions. *Nature Climate Change*, *10*(12), 1130–1136.
- 1376 https://doi.org/10.1038/s41558-020-00920-8
- 1377 Wang, H. (2011). Formation of nascent soot and other condensed-phase materials in flames.
- 1378 Proceedings of the Combustion Institute, 33(1), 41–67.
- 1379 https://doi.org/10.1016/j.proci.2010.09.009
- 1380 Wang, Y., Hu, M., Xu, N., Qin, Y., Wu, Z., Zeng, L., Huang, X., & He, L. (2020). Chemical
- 1381 composition and light absorption of carbonaceous aerosols emitted from crop residue burning:
- 1382 Influence of combustion efficiency. Atmospheric Chemistry and Physics, 20(22), 13721–
- 1383 13734. https://doi.org/10.5194/acp-20-13721-2020
- 1384 Washenfelder, R. A., Attwood, A. R., Brock, C. A., Guo, H., Xu, L., Weber, R. J., Ng, N. L., Allen, H.
- 1385 M., Ayres, B. R., Baumann, K., Cohen, R. C., Draper, D. C., Duffey, K. C., Edgerton, E., Fry, J.
- 1386 L., Hu, W. W., Jimenez, J. L., Palm, B. B., Romer, P., ... Brown, S. S. (2015). Biomass burning
- 1387 dominates brown carbon absorption in the rural southeastern United States. Geophysical
- 1388 Research Letters, 42(2), 653–664. https://doi.org/10.1002/2014GL062444
- 1389 Wilson, D., Dixon, S. D., Artz, R. R. E., Smith, T. E. L., Evans, C. D., Owen, H. J. F., Archer, E., &
- 1390 Renou-Wilson, F. (2015). Derivation of greenhouse gas emission factors for peatlands
- 1391 managed for extraction in the Republic of Ireland and the United Kingdom. *Biogeosciences*,
- 1392 12(18), 5291–5308. https://doi.org/10.5194/bg-12-5291-2015
- 1393 Xie, M., Hays, M. D., & Holder, A. L. (2017). Light-absorbing organic carbon from prescribed and
- 1394 laboratory biomass burning and gasoline vehicle emissions. *Scientific Reports*, 7(1), 7318.
- 1395 https://doi.org/10.1038/s41598-017-06981-8
- 1396 Xie, M., Shen, G., Holder, A. L., Hays, M. D., & Jetter, J. J. (2018). Light absorption of organic
- 1397 carbon emitted from burning wood, charcoal, and kerosene in household cookstoves.
- 1398 Environmental Pollution, 240, 60–67. https://doi.org/10.1016/j.envpol.2018.04.085
- 1399 Xu, Z., Feng, W., Wang, Y., Ye, H., Wang, Y., Liao, H., & Xie, M. (2022). Potential underestimation
- 1400 of ambient brown carbon absorption based on the methanol extraction method and its impacts
- on source analysis. Atmospheric Chemistry and Physics, 22(20), 13739–13752.
- 1402 https://doi.org/10.5194/acp-22-13739-2022
- 1403 Yan, C., Zheng, M., Sullivan, A. P., Bosch, C., Desyaterik, Y., Andersson, A., Li, X., Guo, X., Zhou,
- T., Gustafsson, Ö., & Collett, J. L. (2015). Chemical characteristics and light-absorbing
- property of water-soluble organic carbon in Beijing: Biomass burning contributions.
- 1406 Atmospheric Environment, 121, 4–12. https://doi.org/10.1016/j.atmosenv.2015.05.005
- 1407 Yan, F., Kang, S., Sillanpää, M., Hu, Z., Gao, S., Chen, P., Gautam, S., Reinikainen, S. P., & Li, C.
- 1408 (2020). A new method for extraction of methanol-soluble brown carbon: Implications for
- investigation of its light absorption ability. *Environmental Pollution*, 262.
- 1410 https://doi.org/10.1016/j.envpol.2020.114300
- 1411 Yokelson, R. J., Goode, J. G., Ward, D. E., Susott, R. A., Babbitt, R. E., Wade, D. D., Bertschi, I.,
- 1412 Griffith, D. W. T., & Hao, W. M. (1999). Emissions of formaldehyde, acetic acid, methanol, and

https://doi.org/10.5194/egusphere-2025-2759 Preprint. Discussion started: 26 June 2025 © Author(s) 2025. CC BY 4.0 License.





1413 1414 1415	other trace gases from biomass fires in North Carolina measured by airborne Fourier transform infrared spectroscopy. <i>Journal of Geophysical Research: Atmospheres</i> , <i>104</i> (D23), 30109–30125. https://doi.org/10.1029/1999JD900817
1416 1417 1418 1419	Zhang, Z., Wang, Y., Chen, X., Xu, L., Zheng, Z., Ching, J., Zhu, S., Liu, D., & Li, W. (2025). Absorption enhancement and shielding effect of brown organic coating on black carbon aerosols. <i>Npj Climate and Atmospheric Science</i> , 8(1). https://doi.org/10.1038/s41612-025-00989-y
1420 1421 1422	Zhao, B., Zhuang, Q., Shurpali, N., Köster, K., Berninger, F., & Pumpanen, J. (2021). North American boreal forests are a large carbon source due to wildfires from 1986 to 2016. Scientific Reports, 11(1), 7723. https://doi.org/10.1038/s41598-021-87343-3
1423 1424 1425	Zhong, Q., Schutgens, N., Veraverbeke, S., & van der Werf, G. R. (2024). Increasing aerosol emissions from boreal biomass burning exacerbate Arctic warming. <i>Nature Climate Change</i> , 14(12), 1275–1281. https://doi.org/10.1038/s41558-024-02176-y
1426	